Final Year Project Report

***

Guillaume THIRIET

CI 2018 – Pyrotechnic systems engineering

ENSTA Bretagne

-

Development, measurements and simulation of a micro-combustor for bio-syngas combustion driven thermophotovoltaic power systems

-

26th March 2018 – 17th August 2018

-

Pr. Yueh-Heng Li – Pr. Steven KERAMPRAN

Acknowledgments

First of all, it is a great pleasure to express my deepest thanks and gratitude to **Pr. Yueh-Heng Li** (李約亨), *Professor in the Aeronautics and Astronautics Department of the National Cheng Kung University of Tainan* for proposing the topic of this internship as well as for his supervision, his help during my intern related tasks and his warm welcome. It is a great honour for me to complete my final year project under his supervision within his laboratory in Taiwan.
I also would like to thank my professors **Pr. Steven Kerampran**, **Pr. Michel Arrigoni** and **Pr. Martin Monloubou** for their follow-up during this internship as well as for their teaching and their advice during this last year of studies at ENSTA Bretagne.

Then, I would like to thank my workmates **Davy Sawadogo** and **Chien-Chun Kao** (高建鈞) for their experience sharing, their help during the experiments and their advice all along this internship. It was a great pleasure to work with such amazing people and to help each other to complete our final year project / Master thesis.
In the same way, I wish to address my most sincere thanks to all the students of the laboratory: **Chun-Han Chen**, **Chun-Hsien Lin**, **Chun-Yu Pan**, **Chung-Hao Hsu**, **Ding-Yuan Huang**, **Jie-Wen Li**, **Kai-Lin Xiao**, **Ming-Hsueh Shen**, **Sareddy Kullai Reddy**, **Sunil Kumar**, **Wei-Chieh Kuo**, **Yan-Ru Wang** and **Yu-Ting Yang**, for their welcome, their kindness and their help in daily life as well as in the Chinese understanding. My thankfulness is also to **Clémence Royer**, **Antara Menzel** and **Camille Orth** for their kindness and the French touch within the laboratory.

Finally, I am deeply grateful, and I wish to express my deepest gratitude to **Pr. Guan-Bang Chen** (陳冠邦) for his advice on mastering the StarCCM+® software as well as to **Pr. Fang-Hsien Wu** for her advice and her experienced look on the design of the micro-combustor. I also would like to thank **Mrs. Pascale Ouimette** and **Pr. Ioannis Mantzaras** for the consideration given to my correspondence and their precious advice regarding the combustion simulation for both homogeneous and heterogeneous phase reactions.

Nomenclature

Acronyms	
CFD	Computational Fluid Dynamics
ENSTA	Ecole Nationale Supérieure de Techniques Avancées
GCM	Grid Convergence Method
IR	InfraRed
LIF	Laser Induced Fluorescence
NCKU	National Cheng-Kung University
ODE	Ordinary Differential Equation
PV	PhotoVoltaic
RTE	Radiative Transfer Equation
SCCM	Standard $cm^3.minute^{-1}$
SCTP	Standard Conditions for Temperature and Pressure
SLPM	Standard $liter.minute^{-1}$
TPV	Thermophotovoltaic
ZAP Lab	Zic and Partners laboratory

Greek notations		
$\beta_\lambda(r)$	Extinction coefficient	(1)
Γ	Surface site density	$(mol.m^{-2})$
∇	Differential operator Nabla	***
η	Lamé's coefficient n°1	(Pa)
$\kappa_\lambda(r)$	Absorption coefficient	(1)
λ	Thermal conductivity coefficient	$(W.m^{-1}.K^{-1})$
λ	Wavelength	(m)
μ	Lamé's coefficient n°2	(Pa)
σ_m	Surface site occupancy	$(part.m^{-2})$
ρ	Density	$(kg.m^{-3})$
$\bar{\bar{\tau}}$	Deviatoric stresses tensor	$(Pa.s^{-1})$
$\sigma_\lambda(r)$	Scattering coefficient	(1)
φ	Equivalence Ratio	(1)
ω_k	Volume rate of production of the k^{th} species	$(mol.m^{-3}.s^{-1})$

Notations		
$\bar{\bar{D}}$	Strain rate tensor	(1)
D_k	Thermal diffusivity coefficient of the k^{th} species	$(m^2.s^{-1})$
$\overrightarrow{f_k}$	External body force	$(N.m^{-3})$
h	Enthalpy	(J)
I_λ	The radiant intensity in the Ω direction for a specific wavelength λ	$(W.sr^{-1})$
P	Static pressure	(Pa)
Re	Reynolds number	(1)
$\dot{S}_m$	Catalytic molar production rate of the m^{th} species	$(mole.s^{-1})$
T	Temperature	(K)
T_{Inlet}	Inlet temperature velocity	(K)
t	Time	(s)
U_{Inlet}	Inlet flow velocity	$(m.s^{-1})$
$\vec{v}$	Flow velocity vector field	$(m.s^{-1})$
X_k	Mole fraction of the k^{th} species	(1)
Y_k	Mass fraction of the k^{th} species	(1)

Table of contents

Abstract

The main objective of this research project was to build a reliable numerical model of a new micro-combustor embedding a platinum plate as a catalyst in the middle. The catalytic and the gas-phase combustion reactions of the $H_2/CO/O_2/N_2$ mixture were investigated numerically using the CFD calculation software StarCCM+® while a micro-combustor was designed. Furthermore, the platinum plate was pierced in the middle in order to investigate the influence of the gas-exchanges between the two channels. The presence of a hole on the platinum plate allows the stabilisation of the flame acting as a flame hanger.

The combustion reactions within the micro-combustor involve simultaneously homogeneous phase reactions in the channels as well as heterogeneous phase reactions over the platinum plate. Therefore, prior to build the micro-combustor numerical model, a literature review as well as a study of the main existing mechanisms was pursued in order to identify the more relevant ones as well as the appropriate set of parameters. First, the selected homogeneous phase reaction mechanism was validated reproducing the experimental results extracted from the Mrs. Ouimette Ph.D. Thesis in which different mechanisms for the H_2/CO homogeneous phase combustion reactions were evaluated and compared. Then, the selected heterogeneous phase reaction mechanism was validated reproducing the experimental results extracted from the Zheng et al. (2013) paper in which the catalytic oxidation of carbon monoxide over platinum was experimentally and numerically investigated. An ultimate validation of the two previous mechanisms was carried out by reproducing the experimental results extracted from the Ghermay et al. (2011) and the Schultze et al. (2015) paper about the oxidation reaction of CO in the presence of a $H_2/O_2/N_2$ mixture under different conditions of equivalence ratio and pressure. The micro-combustor numerical model was finally built using the previously defined and validated mechanisms for the homogeneous and heterogeneous phase reactions as well as the associated hypothesis and parameters. The final model as well as the mesh convergence were finally detailed whereas the influence of the inlet mixture composition was numerically investigated.

Along with this numerical study, a new micro-combustor based on the previously engineered one was designed and manufactured in order to solve the sealing defects encountered on the previous model. This new micro-combustor would then be submitted to experiments in order to determine its range of application as well as its efficiency.

Keywords: Micro-combustor, H_2/CO/Air mixture, heterogeneous phase combustion reaction, homogeneous phase combustion reaction, platinum catalysed combustion reaction, Numerical simulation, StarCCM+®

A French and Chinese version of the abstract can be found in appendix n°2.

Introduction

As part of my second year of Master of mechanical and pyrotechnic engineering at ENSTA Bretagne, I carried out my final year project within the combustion and propulsion laboratory of the Aeronautics and astronautics department of the National Cheng-Kung University (NCKU) of Tainan in Taiwan. This final year internship was supervised by Pr. Yueh-Heng Li (李約亨) and took place between the 26th of March 2018 and the 17th of August 2018. The main objective of this final year project was to allow engineering students to lead a true engineering or science project in relative autonomy while having the financial, material and human resources of a company or a research laboratory in order to prepare a future career in the world of engineering and research.
Personally, this final year project was also an opportunity to discover the world of research and therefore to define more deeply my professional project before entering the labour market. It was also a unique opportunity to work in a highly international and multicultural environment since I had the opportunity to interact with people from many different countries with as much different cultural background. In that respect, I trained to converse in English by giving professional oral presentations and courses as well as in Chinese in daily life. In that respect, this final year internship taught me to cope on my own in a country where the culture is very different from the European one while enhancing my language comprehension and speaking skills. Finally, this internship was also the occasion to discover the Chinese culture which was something I wanted to do for a while.

I carried out my final year project within the sub-laboratory “Zic and Partners Laboratory” (ZAP lab) which belongs to the combustion and propulsion laboratory quoted previously. This laboratory is led by the Professor Yueh-Heng Li (李約亨) and focuses its researches on micro-combustion systems, thermophotovoltaic power systems, clean coal combustion technology, biomass energy and electric propulsion. My research project involves the development, testing and simulation of a new concept of micro-combustor embedding a platinum plate for bio-syngas combustion driven thermophotovoltaic power systems. In that respect, I created an associated CFD model using the StarCCM+® calculation software to examine the combustion features under various conditions. This research project belongs to two of the five fields of study of the laboratory: micro-combustion systems and thermophotovoltaic power systems. Moreover, it involves two NCKU second year master students: Davy Sawadogo and Chien-Chun Kao (高建鈞) from Burkina-Faso and Taiwan respectively with whom I collaborated actively during experiments especially but also during numerical calculations and project management.

First, the research project was introduced by a brief state-of-the-art of the micro thermophotovoltaic devices and their interests for a future use in portable and maintenance-free long term off grid power generation systems. Then, the selected homogeneous and heterogeneous phase mechanisms were presented and validated using various numerical models extracted from the literature. This preliminary study was also used to define the most efficient models and set of parameters which need to be used to build a reliable numerical model for the micro-combustor. Finally, the building of the micro-combustor CFD model as well as the associated mesh convergence were detailed. A simple numerical study should have been led varying the inlet gas composition while a campaign of experiments was prepared to determine the range of application of the newly designed micro-combustor.

1. State-of-the-art

Thermophotovoltaics (TPVs) are a highly promising approach to convert heat into electricity via thermal infrared radiation. The heat to electricity conversion process is very close to the usual solar radiation to electricity one. The main difference between both processes relies on the fact that radiation is emitted from a heated body embedding in the TPV device in TPVs' case [Cel – 2011] whereas radiation is emitted by the Sun in the case of a solar power generation device. In the case of TPVs, the emitter is placed very close to the photovoltaic (PV) cells so that the incoming radiation flux density and therefore the power density is close to that of solar PV cells [Zen – 1999] [Yan – 2002]. A scheme of the basic TPV conversion process is shown in figure n°1.

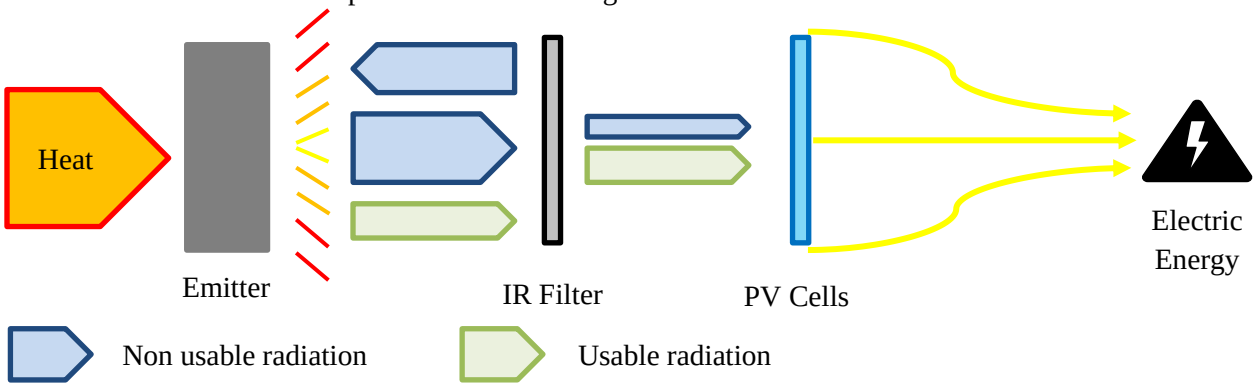

Figure 1: Schematic representation of a TPV device

A basic TPV device is made of:

- A **micro-combustor** / **micro-burner** which produces heat via fuel combustion,
- A **thermal emitter** which receives heat from the micro-combustor and converts it into radiation,
- A **photovoltaic diode cell** which receives radiation coming from the thermal emitter and converts it into electricity.

The **band-pass filter** showed in the figure n°1 is not compulsory to the proper functioning of the TPV device. However, it is highly recommended if a high TPV efficiency is to be reached. The IR band-pass filter transmits the useful radiant infrared energy that is in-band (~1.7 µm to ~0.65 µm) [Hor – 2002] emitted from the incandescent emitter to the PV-cells and reflects the remaining out-of-band radiation to the emitter which will then re-absorb it. The more the IR band-pass filter is efficient, the more it will reflect out-of-band radiation back to the thermal emitter. It is also compulsory to adapt the IR band-pass filter to the characteristics of the PV cells. In that respect, the PV cells only receive radiation whose wavelengths are distributed around the PV cell's peak response which increases PV cells efficiency and deeply decreases energy losses by recycling radiation that PV cells cannot convert into electricity [Hor – 2002]. The use of a well appropriate IR band-pass filter as well as of an efficient design can considerably increase the TPV system efficiency till around 30 % yield which make them highly competitive power generation systems [Hor – 2002].

The thermal emitter can be heated from several different ways. The most common and the one which is studied in this paper is the combustion of fossil fuels or syngas and bio-syngas. These fuels are easy of supply and allow stable and controllable heat sources with a very high energy density which also allow the conception of small-size devices [Kai – 2012] [Wu – 2016] [Yan – 2002]. Solar radiation and radioisotopes [Gri – 1965] can also act as heat-sources for the thermal emitter [Cel – 2011] [Zen – 1999] but they will not be considered here.

However, TPVs' efficiency-cost properties are still pretty weak compared to other power-generating technologies. TPVs are limited in their conversion efficiency by the Carnot efficiency law established in appendix n°6 but mostly by significant heat losses and radical terminations to the walls due to their high surface to volume ratio [Hor – 2002] [NPT – 2018] [Kim – 2006] [Li – 2012] [Yil – 2017]. Indeed, according to the cube-square law, as the size of the combustor is reduced by a factor 100, the surface and the volume will decrease respectively by four and six orders of magnitude respectively. Therefore, the surface to volume ratio will increase by a factor 100 which will considerably increase heat losses and thus the appearance of the quenching phenomenon [Yan – 2002]. In that respect, their fields of use are still limited to the world of research for an application to small-scale power generation systems for portable devices or to solar maintenance-free long term off grid power generation systems [Cel – 2011]. Moreover, usual thermal engines remain far more efficient than TPVs for the power supply of larger devices thanks to their low surface to volume ratio and therefore lower heat losses [Cel – 2011].

The efficiency of a whole very simple TPV device without IR band-pass filter ranges from around 0.5 % to 2.2 % depending of the design of the TPVs as well as of the used materials, TPV cells, the presence of a catalyst… [Cel – 2011]. The performance of such a device relies heavily on the efficiency of the conversion of the radiative energy emitted by the thermal emitter into electricity via the use of PV cells. Usually, it is considered that the electrical conversion efficiency can reach 30 % for solar radiation whereas it only reaches 15% to 20% for the use of natural gas within a TPV device [Hor – 2002]. In that respect, George D. Cody et al. (1999) shows via fundamental calculations that for a black body thermal emitter temperature of 1200 K to 2500 K and $GaSb$ TPV cells, the maximum conversion efficiency varies from 30 % to 35 % and the power density from 5 to 80 W.cm^{-2}. However, these results are overstated, and more reliable numerical models show that the efficiency as well as the power density should be around half of those got with the fundamental calculations [Cod – 1999]. These numerical results are corroborated by Matthias Zenker et al. (1999) for a black body thermal emitter at 1500 K and $GaSb$ TPV cells. In this study, an idealised model shows that the radiation conversion efficiency and the power density are 34 % and 2.2 W.cm^{-2} while a more realistic and reliable model shows that the radiation conversion efficiency and the power density value is 9.1 % and 1.2 W.cm^{-2} respectively [Zen – 1999]. In the same way, Lewis Fraas et al. (1999) shows via experiments that for a SiC (Syralmic 2000) thermal emitter temperature of 1723.15 K and $GaSb$ TPV cells, the radiation conversion efficiency and the power density reach 16.4 % and 2.5 W.cm^{-2} [Fra – 1999]. By the way, it was shown that the efficiency can be enhanced by increasing the temperature to reach about 21 % [Cel – 2011]. However, increasing the temperature also raises thermal stress and can lead to accelerated aging and then to the failure of the TPV device. These results are summarised in the table n°1.

Table 1: Theoretical conversion efficiency and power density for different type of thermal emitter

	Black body thermal emitter 1200 K – 2500 K $GaSb$ TPV cells [Cod – 1999]		**SiC thermal emitter 1723.15 K $GaSb$ TPV cells** [Fra – 1999]	**Black body thermal emitter 1500 K $GaSb$ cells** [Zen – 1999]	
	Fundamental calculations	Numerical models	Experiments	Idealised numerical model	Realistic model
Conversion efficiency (%)	30 - 35	15 – 17.5	16.4	34	9.1
Power density (W.cm^{-2})	5 - 80	2.5 - 40	2.5	2.2	1.2

These power densities must be compared with the current state of art of batteries. The table n°2 shows power densities of batteries assuming that they are functioning for one hour and that one of their dimensions (Length, width, depth) is 1 cm. It appears that TPVs have a power density about twice as large than the best Li-ion batteries.

Table 2: Power density of the main existing type of batteries

	Lead Acid		**NiCd**		**NiMH**		**Li-Ion**	
	Min	Max	Min	Max	Min	Max	Min	Max
Energy Density (Wh/cm^3)	0.06	0.11	0.05	0.15	0.14	0.3	0.25	0.7
Power Density (W/cm^2)	0.06	0.11	0.05	0.15	0.14	0.3	0.25	0.7

Moreover, batteries are also very bulky and heavy which make them quite inappropriate or inconvenient for many applications as low size batteries are not sufficient to supply small-scale devices with long time high density energy power. It can be added that batteries recharging time is pretty long while their operation time between recharging is quite small. In that respect, other sources of power need to be found and, in this context, the use of hydrocarbon fuels or syngas in combustion driven micro-power generation systems such as TPVs devices appears to be very promising [Yan – 2002] [Yan – 2010]. These latter can supply power while maintaining relatively small dimensions and are also easily and quickly refillable by changing the gas cartridges while their operation time remains comparable to that of batteries [Yan – 2010] [Kai – 2012]. From an ecological perspective, although batteries do not reject directly any green-house gases, they often do not last enough and are very difficult to recycle as they are made of heavy metals such as lithium or lead.

By the way, TPVs appear to be very efficient for several classes of problem where standard engines are not usable because they are too expensive to be maintained in operation or not enough reliable [Cel – 2011]. In that respect, they are very interesting devices for long remote missions where highly reliable systems are necessary and in the same way, they are very encouraging devices for portable power-generation systems thanks to their high energy density and therefore their reduced weight and volume [Kai – 2012]. Furthermore, TPVs do not have moving parts [Li – 2013] [Wu – 2016] [Kai – 2012] [Li – 2009] [Yan – 2002] which make them relatively easy to manufacture and very quiet. Then, it also prevents the development of vibrations within the system, preserves the structural integrity and minimises heat dissipation through mechanical friction. In that respect, it considerably decreases the need of maintenance operations [Li – 2009] [Wu – 2016] [Kai – 2012]. Finally, although the electrical conversion of the radiative energy emitted from a thermal emitter heated by the combustion of methane, syngas or bio-syngas is lagged behind the electrical conversion of solar radiation (15-20% using gas combustion / 30% using solar radiation), TPV devices allow 24-hour operation which leads to better efficiency as well as extreme flexibility compared with the usual solar PV cells [Hor – 2002].

In combustion-driven micro-power generation systems, the micro-combustor is with the thermal emitter and the PV cells, one of the main component of a micro-TPV device. In that respect, the efficiency of a TPV device is directly linked to the efficiency of the associated micro-combustor. However, considering the reduced size of the latter, several peculiar issues can appear and need to be solved in order to make micro-combustors and so on TPVs competitive [Lee – 2003]. Among others, the wall effects on the homogeneous phase mechanism are more pronounced due to heterogeneous reactions at the surface and the heat losses to the surrounding walls can also considerably decrease the efficiency of the micro-combustor leading to flame instability and then to thermal quenching [Lee – 2003].

In that respect, considering the major issues that are ecology and power supply, the development, and the application of a micro-combustor for bio-syngas combustion driven portable thermophotovoltaic power system is a very interesting and relevant topic. Nowadays, it prevails to use biomass and urban waste to produce bio-syngas through gasification process as explain in appendix n°5. H_2 and CO are the two main components of bio-syngas far beyond CH_4 but these gases have inherently low heating value compared with the traditional CH_4 [Wal – 2001]. In that respect, the use of catalytic reactions is a feasible solution to enhance the efficiency of such gases and make them competitive with respect to traditional fuels and combustible gases.

In this research project, the combustion characteristics, the flame behaviour as well as the contribution of the catalytic reaction within a micro-combustor embedding a platinum plate as a catalyst in the middle need to be experimentally and numerically studied. The platinum plate allows both heterogeneous and homogeneous combustion reactions and therefore the employment of syngas and bio-syngas for producing thermal energy for TPVs [Kai – 2012] [Sui – 2017]. It also has a hole in order to allow radical exchanges between both channels and then the flame stabilisation. Experimentally, the deployment of a $CO/H_2/Air$ mixture within the micro-combustor is done varying the composition as well as the flow rate to study the combustion process using a direct optical method.

The cylindrical micro-combustor for cylindrical thermophotovoltaic power generation devices was already studied extensively in previous years [Yan – 2002] [Yan – 2010] [Li – 2005] [Li – 2008] [Li – 2013]. This cylindrical design shows to be very limited in terms of modulization and the manufacturing as well as the assembly of the surrounding IR filter and PV cells face some difficulties [Yan – 2010]. In that respect, it is relevant to look after a more convenient design to decrease manufacturing costs and increase efficiency by enhancing modulization. A simplified scheme of a cylindrical micro-combustor is shown on the figure n°2.

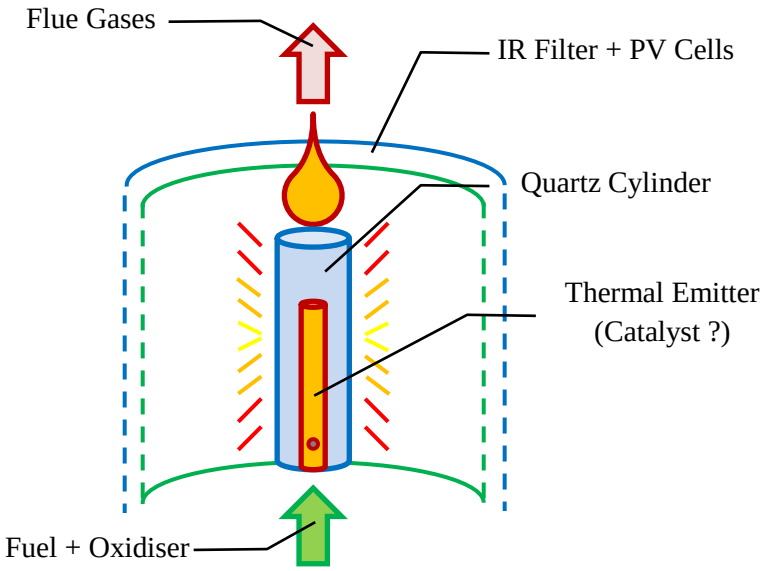

Figure 2: Schematic representation of a cylindrical TPV device

To solve the issues and difficulties encountered with a cylindrical micro-combustor, a rectangular design embedding a platinum plate as a catalyst in the middle was imagined and engineered by the "ZAP Lab" combustion laboratory of Tainan, Taiwan.

- From a pure scientific point of view, this new model of micro-combustor allows to study the efficiency of the rectangular design in comparison with the cylindrical one. As the rectangular design is easier to manufacture than the cylindrical one [Yan – 2010], it allows firstly to reduce manufacturing costs and thus operation costs. Then, it was also shown that rectangle micro-combustor has a much higher radiation efficiency than the micro-cylindrical combustor [Lee – 2003] [Yan – 2010]. This model of micro-combustor would allow to study the combustion reaction and its characteristics as well as the participation of the heterogeneous reactions and the influence of the radical exchanges through the hole on the central platinum plate.

- From a technical point of view, this micro-combustor is intended to be used in series as showed in the figure n°4 to produce enough energy to power a complex mechanical system. This configuration consists in a series of rectangular micro-combustors, planar emitters, filters and PV cells and allows a maximum efficiency as each micro-combustor contributes to the heating of their neighbours, which considerably decreases the risk of flame instabilities as well as thermal quenching by slashing heat losses. The addition of the catalytic combustion as well as a heat recirculation system could also contribute to the enhancement of the micro-combustor performance by limiting the issues previously quoted. A simplified scheme of a rectangular micro-combustor is shown on the figure n°3. This design simplifies greatly the fabrication and assembly process of the whole TPV device while enhancing its efficiency and its flexibility as the adjustment to power requirements only necessitate the addition or the removal of some micro-TPV units.

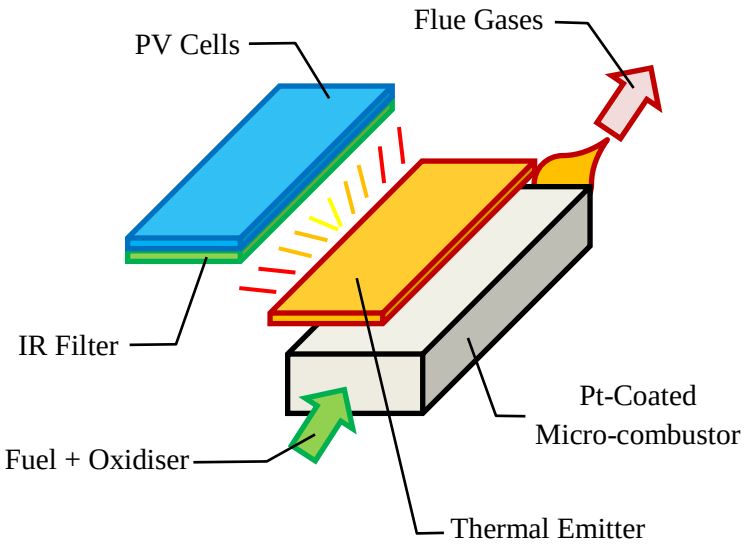

Figure 3: Schematic representation of a modular TPV device

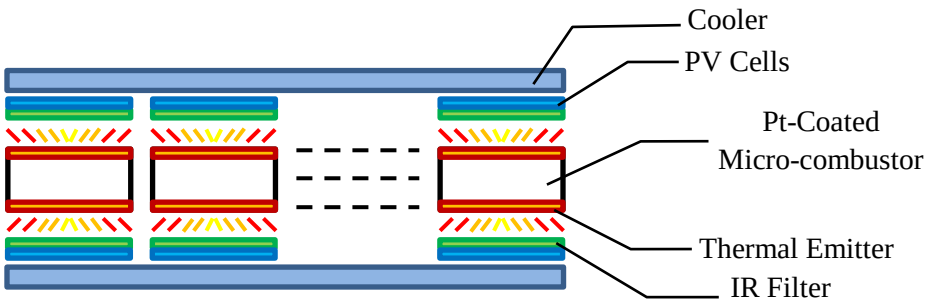

Figure 4: Schematic representation of a series assembly of TPV devices

2. Experimental apparatus

2.1. State-of-the-art on the design of a micro-combustor

Two of the major challenges when designing a micro-combustor for a combustion driven thermophotovoltaic power system is the sustainability of the reaction as well as the maximisation of the radiation output emitted from the thermal emitter [Wu – 2016]. The first challenge stems from the fact that the risk of extinction due to the thermal quenching phenomenon is particularly high in micro-combustor due to their inherent small dimensions. On the one hand, a high surface-to-volume ratio (S/V) is very favourable for output power density per unit of volume but on the other hand, a high heat output may compromise stable combustion. The high heat losses do not only decrease the chemical efficiency of the combustion, but also deactivate chemical reactions by lowering the flame temperature. This phenomenon is explained in detail in appendix n°4. The second challenge depends of course on the efficiency of the thermal emitter but also on the amount of energy released during the combustion process. The design for a new concept of a micro-combustor embedding a drilled platinum plate as a catalyst is proposed herein in order to enhance the energy released using heterogeneous phase reactions in addition to the usual homogeneous phase reactions. It was indeed shown that catalytic micro-combustors have superior stability than homogeneous ones [Kai – 2012].

The following micro-combustor is empirically designed so that it overcomes critical heat loss and prevent thermal quenching as well as flame instabilities. It is used to determine the influence of the heterogeneous combustion reactions stemming from the addition of a platinum plate on the combustion process as well as to study the gas exchanges between the two channels via the hole on the platinum plate. The first objective of this experimental study is to determine the range of application of the newly designed micro-combustor. As explained in the part n°1, micro-combustor requires high power density which can be obtained by increasing the inlet flow rate and thus the inlet velocity. If low flow velocities allow to reach high fuel conversion thanks to high residence time, it was shown that low flow velocities result in insufficient energy input and then to low temperatures due to heat losses and finally to possible extinction due to the thermal quenching phenomenon. On the contrary, high flow velocities result in low residence times whereby the fuel has no sufficient time to react which is called the blowout effect [Li – 2012] [Yil – 2017]. In that respect, the difficulty lies in the design of a micro-combustor balanced between heat losses and small dimensions.

The current design of the micro-combustor is pretty simple, and its efficiency could be slightly enhanced by adding some simple elements to its structure. For instance, the addition of cavities in the flow area can provide recirculation zones and then enhance the flame stability [Yil – 2017]. It was shown through numerical studies that catalyst segmentations and cavities can enhance heterogeneous and homogeneous reactions and more generally extend the stable operating range of catalytic combustion in small-scale combustor for a wide range of inlet flow velocity [Li – 2012]. These latter can also act as heat and radical sources to stabilise the flame and enhance the reaction. In that respect, it solves the issue of short residence time for high velocity flows and compensates the lack of heat in low velocity flows [Li – 2012]. In the same way, a simple backward facing step can be set up at the inlet in order to improve the mixing of the inlet gases by providing a recirculation zone and to enhance the residence time of gases within the micro-combustor [Yil – 2017]. It also allows to control the flame position acting as a flame hanger. The hole on the platinum plate will play a similar role.

2.2. The micro-combustor

The micro-combustor is a major component in the conception of micro-power systems like TPVs. The device used during the campaign of experiments is the micro-combustor V2 whose a 3D view is shown on the table n°3. The use of stainless steel for the design of each sub-parts is compulsory to prevent oxidation due to the combustion process. The platinum is a noble metal and is not concerned by this issue. The micro-combustor (V2) sub-parts are shown and described in appendix n°11. Their detailed blueprints are shown in appendix n°12-13-14-15-16-17-18-19 and 20.

Table 3: 3D view of the micro-combustor V1 and of the micro-combustor V2 (CATIA V5)

Micro-combustor V1 and V2 assembly

Micro-Combustor V1	**Micro-Combustor V2**
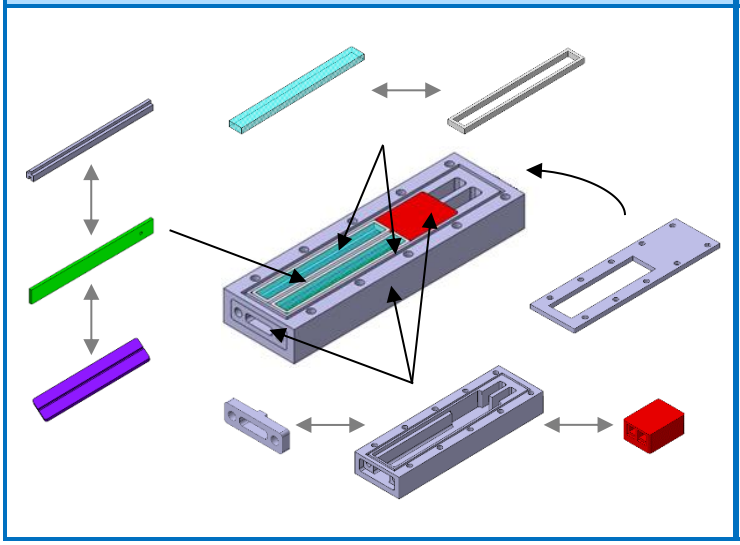	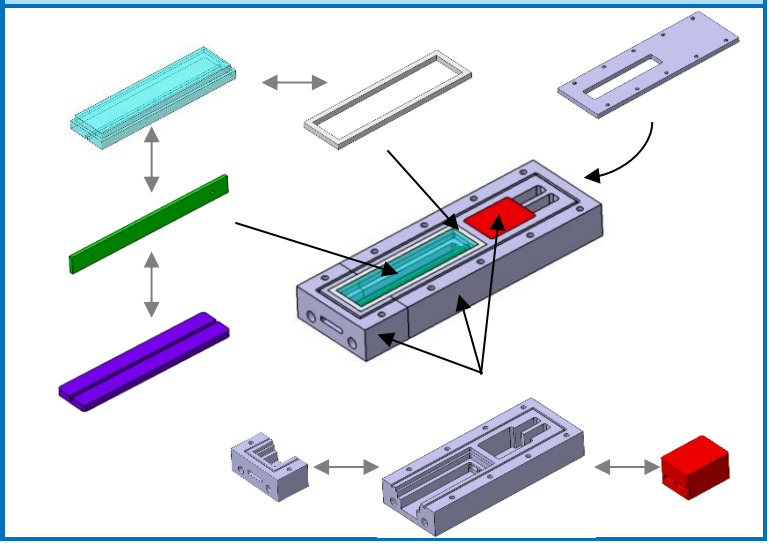

There are two very similar versions for the micro-combustor design. The 1st version (V1) was previously designed by the laboratory but the latter malfunctioned because of a small design error. On the V1 design, the Teflon® seals were in contact with the flame during the combustion process which led to their melt and then their destruction. In that respect, leaks appeared at the junctions between the main body of the micro-combustor and the quartz-plates which then compromised the continuation of the experiments.

To solve this issue, the use of machined carbon graphite plates highly resistant to extreme temperature (> 3000 K) were considered to replace the Teflon® seals. Unfortunately, these latter were brittle and friable which made them impossible to be cut manually to the appropriate dimensions.
The use of a high resistant temperature copper-based silicone (600 K - 800 K) was then considered. But the viscosity of the latter made it very difficult to apply on the very thin slots at the quartz-plates / main body interfaces and the quality of the resulting seals was very approximative. Furthermore, the latter was not resistant enough to the flame temperature and burned slowly dispersing burned silicone powder within the micro-combustor and creating leaks at the quartz-plates / main body interfaces.

Finally, a 2nd version of the micro-combustor (V2) was designed to solve definitively the issue of the flame in contact with the seals inherent to the 1st version of the micro-combustor (V1). The flame temperature of the H_2/CO/Air combustion reaction can reach around 2300 K [Oui – 2012] on the flame axis but this one decreases quickly due to convection and heat losses. By preventing the flame to be in contact with the seals, the use of Teflon® whose melting temperature is about 330 °C [IFA – 2018] can be considered as it was shown empirically that the latter can resist the temperature [Wu – 2016] in similar experimental cases. In that respect, the objective was to design a new micro-combustor whose design should prevent any contact between the flame and the Teflon® seals. The platinum plate had to be kept considering the price of such a metal (platinum price ~2/3 gold price) and the dimensions of the channels of the new micro-combustor should match with the dimensions of the previously designed one.

The decision was taken to replace the two quartz plates and the upper bracket by a unique quartz plate embedding a slot in the middle to maintain the upper side of the platinum plate and therefore to replace the upper bracket function. This choice allowed to reduce the number of interfaces and thus, to remove the risk of leaks on the platinum plate sides. The removal of the upper bracket also greatly improved the visibility of the combustion reaction process near the platinum plate where heterogeneous reactions are predominant as the latter was covering the central part of the channels by about 2 millimeters. The presence of a rectangular staircase shaped location on the top of the main body of the micro-combustor associated with the design of the new quartz-plate prevents any contact between the flame and the seals. In that respect, although the Teflon® melting temperature is around 330 °C [IFA – 2018], the latter can be used as it can be set-up sufficiently far from the flame and protected by stainless steel from the micro-combustor main body and quartz from the quartz plate. The dimension of the seals was doubled which also contributed to enhance its resistance to high temperature.

- **Body – 1:**

The 1st part of the body of the micro combustor is made of stainless steel to avoid oxidation due to the combustion process. It allows the positioning and the fixation of the other sub-parts of the micro-combustor.

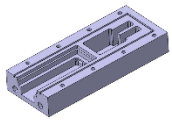

- **Pre-chamber:**

The pre-chamber is made of stainless steel and is maintained inside the micro-combustor body via a same-dimension machined slot. The inside is filled with hollow small copper tubes in order to prevent the flashback hazard using the thermal quenching phenomenon. Furthermore, copper is a very cheap and efficient thermal spreader. The use of such a metal ensures a uniform inlet gas temperature on both side of the platinum plate at lower cost [Cop – 2018]. Its thermal characteristics compared to other metals thermal characteristics are given in appendix n°3.

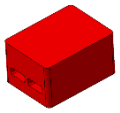

- **Body – 2:**

The 2nd part of the body is made of stainless steel and is fixed to the micro-combustor body using screw fasteners. For machining reason, it was compulsory to manufacture the main body in two separate parts. It suits perfectly with the 1st part of the body and allows to close the micro-combustor. It can be removed to disassemble the device.

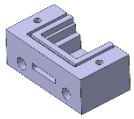

- **Bottom bracket:**

The bottom bracket is made of stainless steel. Its role consists in keeping the platinum plate straight within the micro-combustor. An upper bracket made of stainless steel / a slot in the quartz plate for the micro-combustor V1 / V2 respectively allows to maintain the upper side of the platinum plate as well as to definitively separates the two channels.

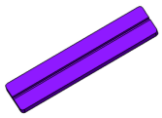

- **Platinum plate:**

The platinum plate role consists in catalysing the combustion reaction by involving heterogenous phase reactions with the H_2/CO fuel mixture. There are two different platinum plates. The first one is a full rectangle platinum plate of 50mm*5mm*1mm dimensions whereas the second one involves a 1mm diameter hole located at 5 mm of the plate extremity at half the width of the plate.

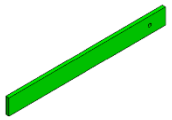

- **Quartz plate:**

The quartz plate is maintained to the micro-combustor main body using a same dimension Teflon® seal. It allows the observation of the combustion process within the micro-combustor and to maintain the platinum straight via a thin slot machined to fit the platinum plate dimensions. On the micro-combustor V1, the quartz plate was replaced by two separate rectangular quartz-plates.

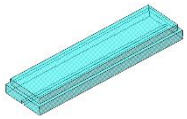

- **Teflon/Carbon seal:**

The seal surrounding the upper quartz plate prevents leaks between the outside environment and the inside of the micro-combustor at the quartz plate/micro-combustor body junction. It is made of Teflon® to fit inside the slot machined on the micro-combustor main body and is maintained by the upper cover plate which is used to close the upper side of the micro-combustor. The Teflon® is not highly resistant to high temperature so it is compulsory to prevent any contact between the latter and the flame.

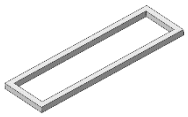

- **Upper cover plate:**

The upper cover plate is made of stainless steel and is used to close and seal the micro-combustor body as well as the micro-combustor sub-parts using screw fasteners.

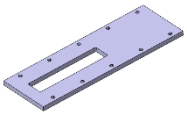

2.3. The experimental setup

A scheme of the simple preliminary experimental setup is displayed on the figure n°5. During the experiments, high purity H_2, CO and Air gases were supplied from pressurised tanks via airtight pipes and connectors. The tightness of the driving device was checked with soapy water which allowed bubble appearance in the presence of gas-leaks. Their flow-rates were monitored via three / four pre-calibrated flow controllers whose reference is given in appendix n°7 and n°8. The calibration method of the flow-controllers is of paramount importance to realise very accurate and reliable experiments. The calibration method is described in detail in appendix n°9.

The micro-combustor used in experiments is the version V2 of the table n°3. In order to ease catalytic ignition and reaction, the micro-combustor was pre-heated to 500 K in an electric hoven [Sui – 2017] before each experiment. The scheme showed on the figure n°5 is there as an example. The configuration can be modified depending on the study to be conducted.

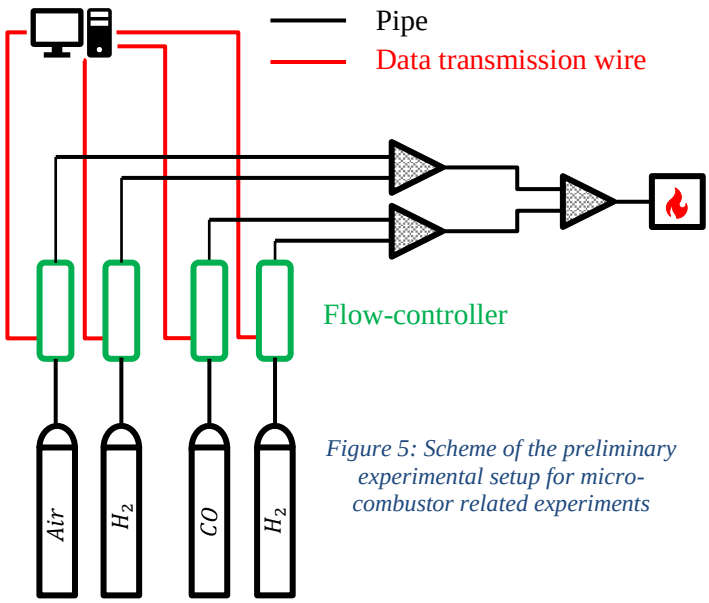

Figure 5: Scheme of the preliminary experimental setup for micro-combustor related experiments

3. Chemical mechanisms

This brief literature review introduces and presents the main existing mechanisms for the $H_2/CO/Air$ homogeneous and heterogeneous combustion reactions. This is by no means an exhaustive list and the reader should be aware that it exists many others different mechanisms for the homogeneous combustion reaction of the $H_2/CO/Air$ mixture, each with their own field of application and specificities. For more information about the $H_2/CO/Air$ homogeneous mechanisms, the reader is asked to refer to the Mrs. Ouimette PhD. Thesis [Oui – 2012] (In French) in which many different mechanisms for the homogeneous combustion reaction are presented and detailed or to the associated references. The main homogeneous mechanisms are numerically compared to evaluate the influence of their differences on the numerical results in the case of a steady state, simple laminar, partially-premixed flame.

The first efficient and comprehensive kinetic mechanism for the $H_2/CO/O_2$ homogeneous combustion reaction was developed and published by Yetter et al. (1991) [Yet – 1991] and hold 13 different species as well as 28 reactions. This first mechanism was already efficient to describe the combustion process on a wide range of temperature, mixture composition and pressure. Then, this homogeneous combustion mechanism was regularly updated by new mechanisms enhancing step by step the elementary chemical reactions as well as the related Arrhenius kinetic constants. Mueller et al. (1999) [Mue – 1999] upgraded the Yetter et al. (1991) mechanism by including the chemical reactions for the formation of NO_x whereas Li et al. (2007) [Li – 2007] extended the mechanism to C1 species such as CO, CH_2O and CH_2OH. These two mechanisms hold respectively 21 different species, 66 reactions and 13 different species, 36 reactions. Afterwards, Davis et al. (2005) [Dav – 2005] published an optimised mechanism based on the Mueller et al. (1999) one holding 14 different species and 38 reactions. This simpler optimised mechanism was then enhanced by Sun et al. (2007) [Sun – 2007], Li et al. (2007) and Sung et al. (2008) [Sung – 2008] whose mechanisms hold respectively 33, 36 and 30 reactions. These three mechanisms are now considered as references for the numerical study of the $H_2/CO/Air$ homogeneous combustion reaction. Finally, Boivin et al. (2011) [Boi – 2011] published a highly reduced mechanism holding 12 different species (14 including He and Ar) as well as 16 reactions. Although greatly reduced, this mechanism allowed to decrease the calculation time while keeping the quality of the predictions got with more sophisticated and complete mechanism [Oui – 2012].
The GRI-Mech 3.0 [Smi – 2018] is another very complete kinetic mechanism designed to model the homogeneous reaction of the CH_4/H_2 mixture. It was designed by the combustion department of the Berkeley university and included the NO_x as well as other pollutants formation kinetic mechanisms. Although it applies preferentially to the combustion reaction of natural gas, it can also be used with a very good accuracy to model the reaction of syngas made of H_2/CO. However, considering the low computing power, the complexity of the mechanism and the fact that simpler efficient mechanisms for the $H_2/CO/Air$ combustion reaction were developed, it is not studied there.

The literature review showed that although many different mechanisms for the homogeneous phase combustion reaction of the $H_2/CO/Air$ syngas mixture were developed, the opportunity to enhance the combustion characteristics of such a mixture using platinum (Pt) as a catalyst was somewhat left out by researchers. Pr. Mantzaras is one of those who pursued experimental and numerical studies on the catalytic combustion of syngas/air mixtures over platinum enhancing the heterogeneous mechanism of Deutschmann et al. (2000) developed to model the heterogeneous reaction of the $H_2/CO/CH_4$ mixture on Pt. He ran numerical calculations about the platinum catalysed combustion reaction of the $H_2/CO/Air$ mixture representative of the syngas composition using streamlined

chemical mechanisms for the homogeneous and heterogeneous phase combustion reactions [Man – 2008].

Whatever it might be and for every mechanism mentioned above, the reaction rate kinetic parameters were mainly extracted from Warnatz et al. (1984) [War1 – 1984] [War2 – 2006]. However, most of them were modified and upgraded to consider the publication of more recent papers and studies. Their evolution is not detailed here. The main studied homogeneous mechanisms are detailed in the table n°4.

Table 4: Synthesis of the main existing mechanisms for the CO/H_2/Air homogeneous combustion reaction

	Main Homogeneous Phase Mechanisms	
	Number of species	**Number of reactions**
GRI-Mech 3.0 [Smi – 2018]	53 (Including Ar)	325
Davis et al. (2005) [Dav – 2005]	14 (Including Ar and He)	38
Mantzaras (2008) [Man – 2008]	13	33
Boivin et al. (2011) [Boi – 2011]	14 (Including Ar and He)	16

The selected homogeneous mechanism was extracted from the Mantzaras et al. (2008) paper [Man – 2008] and adapted from the Sun et al. (2007) [Sun – 2007] and Davis et al. (2005) [Dav – 2005] mechanisms. Several minor duplicate reactions as well as the less predominant reactions were removed to simplify the mechanism as showed in appendix n°27. Furthermore, if the kinetic parameters were mainly extracted from Warnatz et al. [War1 – 1984] [War2 – 2006], several minor changes on the Arrhenius coefficients were made to consider the removal of the least predominant reactions aforementioned. To sum up, the Pr. Mantzaras homogeneous mechanism is a streamlined version of the reference homogeneous mechanisms of Sun et al. (2007). and Davis et al. (2005) and would allow to lead precise calculation while saving some computing time as showed thereafter.

The selected heterogeneous phase mechanism was extracted from the Mantzaras et al. (2008) paper [Man – 2008] and adapted from the Deutschmann et al. (2000) heterogeneous mechanism [Deu – 2000] which reproduces precisely the ignition and the steady combustion reaction of the $H_2/CO/CH_4$ mixture on Pt. Methane related reactions were removed as they were not relevant for the current study. As well as for the homogeneous phase reaction mechanism, the surface thermodynamic data were mainly extracted from Warnatz et al. [War1 – 1984] [War2 – 2006] and then modified using more recent papers [Zhe – 2013]. The reactions involving the $HCOO(s)$ species highlighted in the table n°5 were added as it was shown that these latter can have a significant impact on the numerical results for some specific conditions of temperature and pressure. The surface site density was fixed to $\Gamma = 2.7 * 10^{-9}$ mol.cm^{-2} [Deu – 2000] [Man – 2008] [Zhe – 2013].

Table 5: The HCOO(s) related reactions and their Arrhenius kinetic coefficients [Zhe - 2013]

***The HCOO(s) related reactions and their Arrhenius kinetic coefficients* [Zhe – 2013]**			
	A	**n**	**E_a (J.mol^{-1})**
$OH(s) + CO(s) \longrightarrow HCOO(s) + Pt(s)$	3.70E+21	0.0	94,200
$HCOO(s) + Pt(s) \longrightarrow OH(s) + CO(s)$	1.33E+21	0.0	870
$HCOO(s) + O(s) \longrightarrow OH(s) + CO_2(s)$	3.70E+21	0.0	0.0
$OH(s) + CO_2(s) \longrightarrow HCOO(s) + O(s)$	2.79E+21	0.0	151,050
$HCOO(s) + Pt(s) \longrightarrow CO_2(s) + H(s)$	3.7E+21	0.0	0.0
$CO_2(s) + H(s) \longrightarrow HCOO(s) + Pt(s)$	2.79E+21	0.0	90,050

It is shown in appendix n°27 that the numerical results got with the Davis et al. (2005), Mantzaras et al. (2008) and Boivin et al. (2001) homogeneous mechanisms were very close whether on the temperature radial profile or on the species mole fraction profile. However, the time calculation required to compute these results varies significantly due to the number of elementary steps as well as to the used model. In that respect, the Davis et al. (2005) mechanism is the longest one. It is followed by the Mantzaras et al. (2008) mechanism which is **14 % / 27 %** faster using the Mass-Weighted Mixture / Mathur-Saxena Averaging model respectively and then by the Boivin et al. (2011) mechanism which is **26 % / 28 %** faster using the Mass-Weighted Mixture / Mathur-Saxena Averaging model respectively. The Total Solver CPU Time values are summed-up in the table n°6.

Table 6: Total solver CPU time for the Davis, Mantzaras and Boivin's mechanism

Total solver CPU time for the Davis, Mantzaras and Boivin's mechanism		
	Mass-Weighted Mixture	**Mathur-Saxena Averaging**
***Davis et al.* (2005)**	1	1
***Mantzaras et al.* (2008)**	0.86	0.73
***Boivin et al.* (2011)**	0.75	0.72

Finally, considering the very close results got for the temperature and the species mole fraction profiles with the three different mechanisms, their associated computing time as well as for purposes of consistency, the Pr. Mantzaras' mechanisms for the homogeneous and heterogeneous combustion reactions were selected to be used in the following numerical calculations. The selected homogeneous mechanism is a good streamlined gas-phase mechanism whereas the heterogeneous mechanism is an adapted version of the heterogeneous reference mechanism for the $H_2/CO/CH_4$ on Pt published by Deutschmann et al. (2000). Both would produce very precise results within a reasonable time. These two mechanisms are summed up in the table n°7 and detailed in appendix n°24 and n°26.

Table 7: Description of the Mantzaras' homo-/heterogeneous phase combustion mechanism

Description of the Mantzaras' homo-/heterogeneous phase combustion mechanism		
Homogeneous phase Mechanism [Man – 2008]	13 species	33 reactions
Heterogeneous phase Mechanism [Zhe – 2013]	13 species	27 reactions

It is important to note that even with a large catalytic platinum surface, the homogeneous reactions cannot be neglected especially at high pressure and temperature [Man – 2008]. In that respect, the modelling of the catalytic combustion of syngas at standard temperature and pressure would involve both homogeneous and heterogeneous reactions. An exception can be made if the equivalence ratio of the mixture is too low to support homogeneous phase reactions [Zhe – 2013]. The Davis et al. (2005), the Mantzaras et al. (2008) as well as the Boivin et al. (2011), homogeneous/heterogeneous mechanisms are shown in appendix n°23-24 and 25.

4. Numerical model

In the whole following numerical study, numerical calculations were run using the commercial fluid dynamics computation software StarCCM+® (2010) based on the finite volume method [Sta – 2016]. The final objectives of the works presented here were to study the behaviour of the flame within the micro-combustor as well as different parameters such as the flame temperature, the gas-flow velocity and the radicals rate of presence under the assumption of steady state in order to improve the micro-combustor design.

4.1. Fundamental reactive Navier-Stokes equations

In order to model and compute the combustion phenomenon of a premixed flame of $H_2/CO/\ Air$ for a laminar or a turbulent flow, the conservative equations of mass, momentum, energy and chemical species should be solved. These equations are presented thereafter [Ker – 2018].

- **The mass conservation equation**

$$\frac{\partial \rho}{\partial t} + div(\rho \vec{v}) = 0 \quad [1]$$

ρ: Fluid density (kg.m^{-3});
$\vec{v}$: Flow velocity vector field (m.s^{-1});
t: Time (s).

- **The momentum conservation equation**

$$\rho \frac{\partial \vec{v}}{\partial t} + \rho \overline{\overline{grad}}(\vec{v})\vec{v} + \overrightarrow{grad}(P) - div\left(\eta div(\vec{v})\bar{\bar{I}} + 2\mu\bar{\bar{D}}\right) = \sum_{k=1}^{n} \rho Y_k \overrightarrow{f_k} \quad [2]$$

P: Static pressure (Pa);
$\bar{\bar{\tau}} = \eta div(\vec{v})\bar{\bar{I}} + 2\mu\bar{\bar{D}}$: Deviatoric stresses tensor (~Viscosity);
$\bar{\bar{D}} = \frac{1}{2}\left(\overline{\overline{grad}}(\vec{v}) + \overline{\overline{grad_T}}(\vec{v})\right)$: Strain rate tensor
$\kappa = \eta + \frac{2}{3}\mu = 0$: Stokes hypothesis
μ: First coefficient of viscosity - η: Second coefficient of viscosity $\Longrightarrow$ Lamé's coefficients (Pa);
$\begin{cases}\mu = 0 \\ \eta = 0\end{cases} \Leftrightarrow$ Inviscid fluid
Y_k: Mass fraction;
$\overrightarrow{f_k}$: External body forces (N.m^{-3}).

- **The energy conservation equation**

$$\rho \frac{Dh}{Dt} + div\left(\rho \sum_k Y_k h_k \overrightarrow{v_{d,k}} - \lambda \overrightarrow{grad}(T)\right) = \frac{DP}{Dt} + \bar{\bar{\tau}} : \overline{\overline{grad}}(\vec{v}) \quad [3]$$

h: Enthalpy (J);
$-\lambda \overrightarrow{grad}(T)$: Fourier heat conduction equation;
λ: Thermal conductivity coefficient (W.m^{-1}.K^{-1})
$Y_k h_k \overrightarrow{v_{d,k}} = -h_k D_k \nabla Y_k$: Diffusive laminar flow of the kth species enthalpy;
D_k: Thermal diffusivity coefficient of the kth species (m^2.s^{-1})
∇: Differential operator Nabla
Y_k: Mass fraction of the kth species (1).

- **The species conservation equation**

$$\rho \frac{\partial Y_k}{\partial t} + \rho \vec{v}.\overrightarrow{grad}(Y_k) + div\left(\rho Y_k \vec{v}_{d,k}\right) = \omega_k \quad [4]$$

$\rho Y_k \overrightarrow{v_{d,k}} = -\rho D_k \overrightarrow{grad}(Y_k)$: Diffusive laminar flow of the k[th] species;
ω_k: Volume rate of production of the k[th] species (Algebraic value) (mol.m^{-3}.s^{-1}).

- **The surface species coverage**

$$\sigma_m \frac{\dot{S}_m}{\Gamma} = 0 \qquad m = 1, \dots, M_s \qquad [5]$$

σ_m: Surface species site occupancy (particule.m^{-2});
$\dot{S}_m$: Catalytic molar production rate of the m[th] species (mol.s^{-1});
$\Gamma = 2.7 * 10^{-9}$: Surface site density (mol.cm^{-2}).

- **The radiative transfer equation**

In order to simplify the problem, the radiation properties of the media as well as of the surrounding surfaces were considered invariant with wavelength. In that respect, the radiation was said to be grey and was modelled by the *Grey Thermal Radiation* model which means that only a single radiative transfer solution was required for the full thermal spectrum. The model used to compute the radiant intensity was the *Participating Media Radiation* whose the formulation using the radiative transfer equation (RTE) is detailed thereafter [Sta – 2016]. The surface properties of emissivity, reflectivity and transmittivity are set to 1, 0 and 0 respectively for the boundaries.

$$\frac{\mathrm{d}I_\lambda(r,s)}{\mathrm{d}s} = -\beta_\lambda(r) I_\lambda(r,s) + \kappa_\lambda(r) I_{b\lambda}(r) + \frac{\sigma_\lambda(r)}{4\pi} \int_0^{4\pi} I_\lambda(\Omega)\, \mathrm{d}\Omega \qquad [6]$$

The change in $I_\lambda(r,s)$ over a differential distance in the s direction

The loss to the medium due to absorption or scattering

The local emission

The contribution to the intensity in the s direction resulting from the scattering of intensity in other direction

Where,
I_λ: The radiant intensity in the Ω direction for a specific wavelength λ.

$$I_{b\lambda} = \frac{2C_1}{n^2 \lambda^5 \left(e^{C_2/n\lambda T} - 1\right)} \qquad \begin{cases} C_1 = 0.595522 * 10^{-16}\ W.m^2.s^{-1} \\ C_2 = 0.01439\ m.K \end{cases}$$

$$\beta_\lambda(r) = \kappa_\lambda(r) + \sigma_\lambda(r) \qquad \begin{cases} \beta_\lambda(r) : \text{The extinction coefficient} \\ \kappa_\lambda(r) : \text{The absorption coefficient} \\ \sigma_\lambda(r) : \text{The scattering coefficient} \end{cases}$$

$\kappa_{a\lambda} = \sum_i \kappa_{a\lambda i}$ with i a gas component

$$s = \sin(\theta)\cos(\phi)\,\vec{\imath} + \sin(\theta)\sin(\phi)\,\vec{\jmath} + \cos(\theta)\,\vec{k}$$
$$d\Omega = \sin(\theta)\, d\theta d\phi$$

The in-scattering coefficient was there assumed to be isotropic. The absorption, the scattering coefficients as well as the refractive index of the medium were there independent of wavelength as the *Grey Thermal Radiation* model was considered.

4.2. Computing power

Numerical calculations were run using a computer embedding four logical quad-core processors Intel® Core™ i5-7500 CPU with 3.40 GHz frequency each.

5. Validation of the chemical mechanisms

Before to set up a complete numerical model of the micro-combustor embedding a platinum plate and run simulations, it is necessary to validate independently the selected mechanisms for the homogeneous phase reaction as well as for the heterogeneous phase reaction. In that respect, preliminary combustion simulations of numerical models extracted from pre-selected papers were firstly run and the associated experimental results were compared to the numerical results. For coherence and efficiency purposes, the selected homogeneous and heterogeneous phase mechanisms are those published by Pr. Mantzaras [Man – 2008] [Zhe – 2013] and inspired by the Davis et al. [Dav – 2005] and the Deutschmann et al. (2000) mechanism [Deu – 2000] respectively as explained in the part n°3.

5.1. Validation of the homogeneous phase mechanism

The numerical model as well as the mesh were extracted from the Mrs. Ouimette Ph.D. thesis [Oui – 2012] in which different combustion mechanisms for the $H_2/CO/Air$ reaction usually used in the literature were presented, studied and compared. In this paper, Mrs. Ouimette developed a simple 2D-numerical model of the partially-premixed laminar flame ($Re = 522$) for a mixture of 50% H_2 / 50% CO with an equivalence ratio $\varphi = 3$ with air as oxidizer $\left(Y_{H_2} = 0.0266, Y_{CO} = 0.3694, Y_{O_2} = 0.1407, Y_{N_2} = 0.4633\right)$. This study showed that a reduced mechanism allowed to reduce considerably time calculation while preserving the quality and the reliability of predictions got with more complex mechanisms. Mrs Ouimette's simulations was processed using FLUENT® 6.3.

In order to allow relevant and reliable comparison between the numerical results and those extracted from the Ph.D. thesis of Mrs. Ouimette, the geometry design, the boundaries, the initial conditions, the mesh as well as the physical model and the hypothesis were reproduced as far as possible. The complete description of the model and underlying assumptions is displayed in appendix n°21. The homogeneous phase mechanism applied consists of an improved version of the Davis et al. (2005) homogeneous phase mechanism for the $CO/H_2/Air$ combustion reactions [Dav – 2005] and was published in the Mantzaras et al. (2008) paper [Man – 2008]. The results are considered convergent as soon as the residuals for each solved equation decrease under 1.10^{-4} which match with about 20 000 iterations.

5.1.1. Geometry and boundary conditions

The geometry used is described in the figure n°6. Assuming that in the steady state, the flame shape is axisymmetric in relation to its longitudinal axis, the geometry can be reduced to a simple rectangle geometry representing a half of the whole physical fluid domain to slash time calculation. The domain is 25.4 mm width which corresponds to twice the burner radius and 100 mm long which represents approximately twice the height of the flame [Oui – 2012]. The fluid domain is split in nine parts which represent nine different levels of refinement of the mesh.

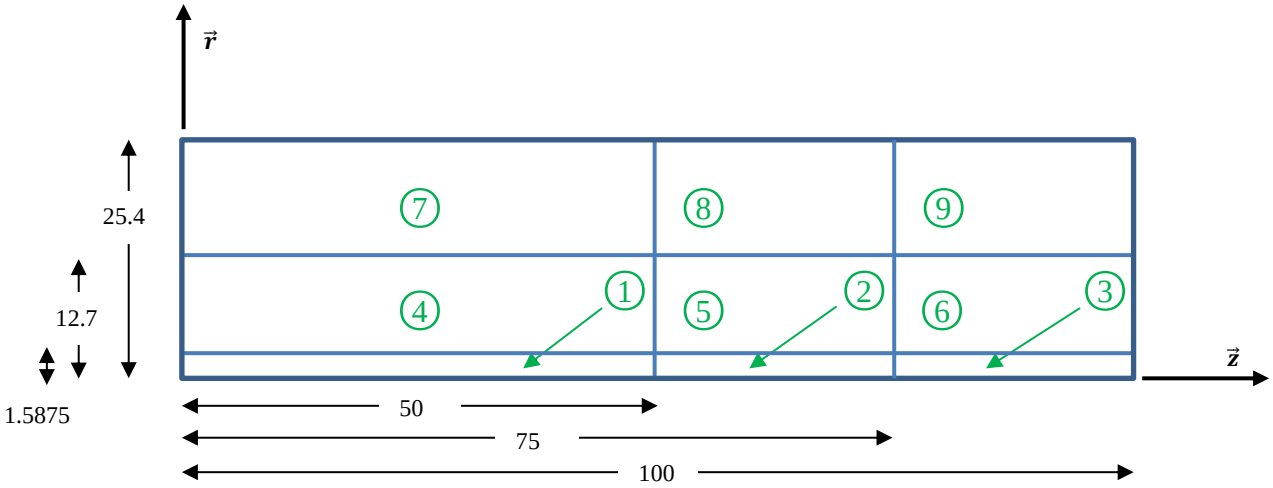

Figure 6: Geometry of the fluid domain used for the validation of the homogeneous phase combustion mechanism [Oui – 2012]

The boundaries of the fluid domain defined previously are described in the figure n°7. The central line of the fluid domain (Dotted line) corresponds to a symmetry axis which means that a zero-gradient value $\left(\frac{\partial \phi}{\partial r}\right)$ is applied for all variables. The boundaries with the outside domain (Dashed line) were chosen to "Pressure Outlet" with a pressure, a temperature and a gas composition which matched with the standard atmospheric conditions. Then, the boundary of the burner wall (Continuous line) was chosen to "Wall" with the *adiabatic*, *impermeable* and *no-slip* specifications for the thermal, the species gradient and the shear stress specification respectively. Finally, the boundary of the injector was chosen to "Velocity Inlet" and the flow specification was defined as follows: the mixture composition is 50% H_2 / 50% CO with an equivalence ratio $\varphi = 3$ with air as oxidizer $\left(Y_{H_2} = 0.0266, Y_{CO} = 0.3694, Y_{O_2} = 0.1407, Y_{N_2} = 0.4633\right)$. The flow velocity was fixed to an axial average velocity $\overrightarrow{u_Z} \cong 3.2$ m.s^{-1} with a fully-developed profile and a radial velocity $\overrightarrow{u_r} = 0$ m.s^{-1} as detailed in appendix n°10.

The initial conditions within and outside the domain matches with the standard atmospheric conditions:

- P = 101325 Pa
- T = 300 K
- $Y_k = \begin{cases} O_2 = 0.2321 \\ N_2 = 0.7679 \end{cases}$

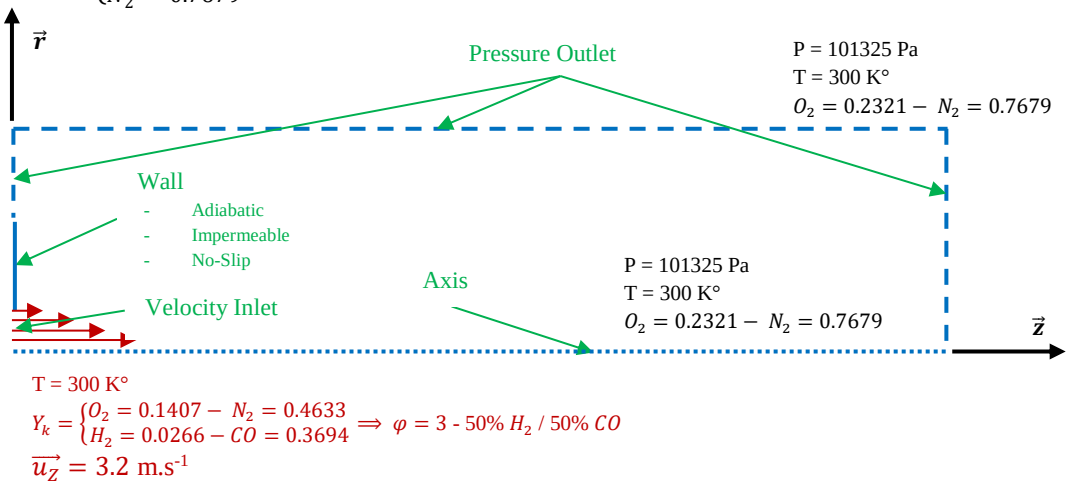

Figure 7: Boundary conditions of the fluid domain used for the validation of the homogeneous phase combustion mechanism [Oui – 2012]

5.1.2. Mesh

The mesh applied on the fluid domain is described in the figure n°8. The fluid domain was split into nine divisions as showed in the figure n°6. The mesh convergence was realised by Mrs. Ouimette in her Ph.D. thesis and therefore, it is not studied here. The cell size for each different section is a constant and fixed by the grid refinement.

The first section is divided using a 15 segments grid on the $\vec{r}$ axis and a 475 segments grid on the $\vec{z}$ axis. In this section, cells are squares each one 0.1 mm in size.

- The sections n°2 and n°3 are divided using the same 15 segments grid on the $\vec{r}$ axis and a 150 segments grid on the $\vec{z}$ axis for the section n°2 and a 75 segments grid on the $\vec{z}$ axis for the section n°3.
- The sections from n°4 to n°9 are divided using the same grid on the $\vec{z}$ axis than the one used for sections n°1, n°2 and n°3. On the $\vec{r}$ axis, the sections n°4, n°5 and n°6 are divided using a 75 segments grid whereas the sections n°7, n°8 and n°9 are divided using a 50 segments grid.

To sum up, the fluid domain was divided into $140 * 700$ cells. In the $\vec{r}$ (Radial) direction, the minimum size of the mesh is 0.1 mm next to the burner whereas the maximum size is 0.25 mm at the border of the domain. In the $\vec{z}$ (Axial) direction, the minimum size of the mesh is 0.1 mm next to the burner whereas the maximum size is 0.33 mm at the border of the domain.

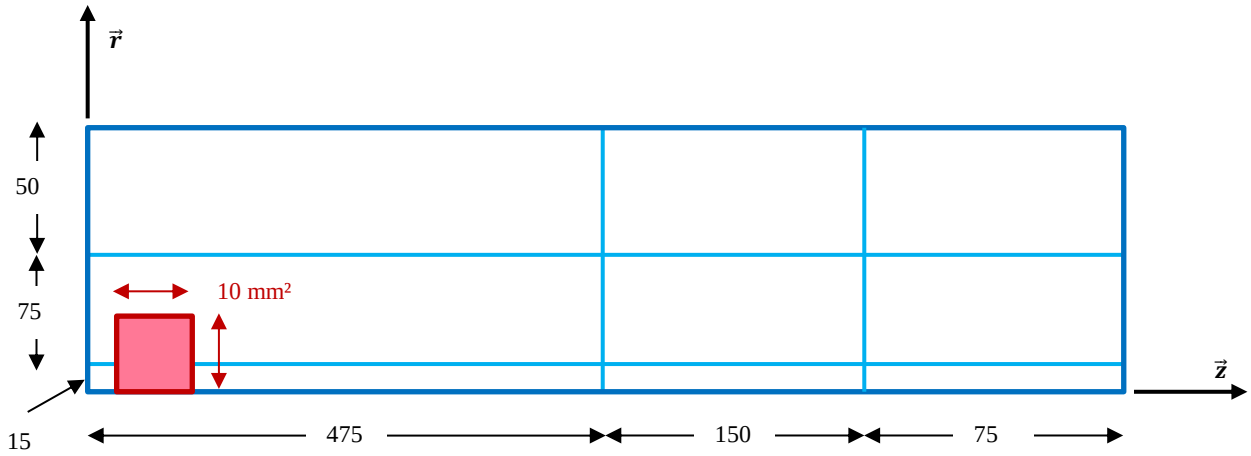

Figure 8: Mesh and ignitor position of the fluid domain used for the validation of the homogeneous phase combustion mechanism [Oui – 2012]

5.1.3. Ignition method

Combustion simulations of the $H_2/CO/Air$ mixture were triggered by igniting the mixture using the "ignitors" option. A temperature of 1500 K is attributed to a 100 mm² square area of the fluid domain located at 1 mm from the burner outlet as illustrated in the figure n°8. This ignitor operates as a "pulse". It is triggered at the 20th iteration and remains active till the 40th iteration. The ignition is instantaneous, and the combustion is then auto-sustained by the elevate temperature and the presence of active radicals once the ignitor turned off.

5.1.4. Results

Cold flow validation

In this part, the inlet flow mixture was not ignited and just flowed out of the burner outlet. The numerical axial flow velocity profile got via the StarCCM+® simulation was compared to the numerical and experimental results displayed in the Mrs. Ouimette's Ph.D. thesis in order to run the following reactive simulations with an appropriate fully developed flow velocity profile. The calculation of the fully developed flow velocity profile is detailed in appendix n°10 [Unk - 2004].

Table 8: Validation of the axial cold-flow velocity profile

Axial flow velocity profile - Mechanism of Mantzaras	
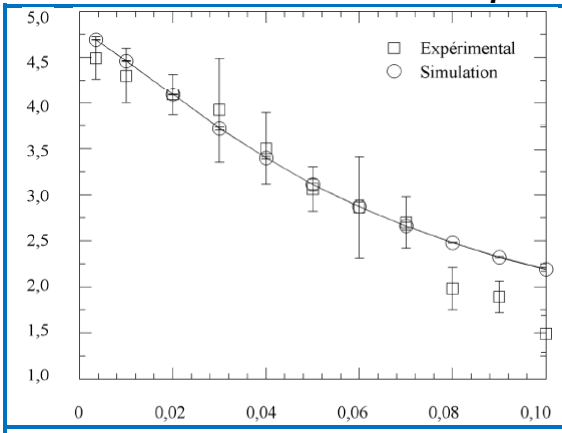	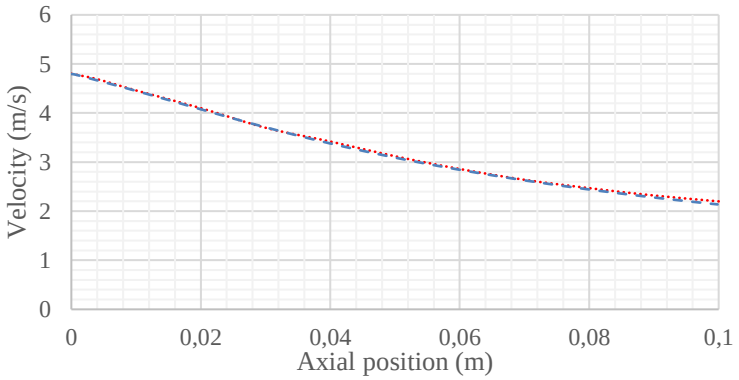
Mrs. Ouimette [Oui – 2012] cold flow axial velocity profile ○: Experimental Results -: Numerical Results	*Pr. Mantzaras* [Man – 2008] cold flow axial velocity profile Mantzaras mechanism numerical results Mrs. Ouimette numerical results

The numerical results for the axial flow velocity profile match very accurately with the numerical results got with FLUENT® 6.3 and published in the Mrs. Ouimette Ph.D. thesis [Oui – 2012]. In that respect, the numerical results also match with the associated experimental measurements of the axial cold flow velocity showed in the table n°8. This validates the use of the equation n°D.1 for the description of the fully-developed velocity profile.

Ignited flow validation

The validation of the ignited flow model was achieved focusing on three physical properties: the flame height, the temperature profile and the species mole fraction profiles. The numerical temperature and the species mole fraction profiles were compared to the Mrs. Ouimette's Ph.D. thesis experimental results. These latter are shown in appendix n°28 and n°29. The numerical model for the validation of the homogeneous combustion reactions mechanism was built step by step as summed-up in the figure n°9.

It is shown in appendix n°28 that the use of the *mass-weighted mixture* model for the dynamic viscosity as well as for the thermal conductivity is far less efficient than the use of the *Mathur-Saxena Averaging* model to simulate the homogeneous combustion reaction of the CO/H_2 mixture. This result is not so surprising as it is not so common that a mixture physical property stems from the weighted average of the physical property of its components.

- The ***Mathur-Saxena Averaging*** model is used in the following simulations.

Then, it is shown in appendix n°28 and n°29 that the influence of the *radiation* on the homogeneous combustion reaction is not neglectable as it allows to reduce the maximum temperature by about **11 %** and to get closer to the experimental results. If the effect of radiation is not neglectable in the case of the homogeneous phase combustion reaction in an open environment, its effect is greatly reduced when the homogeneous reaction takes place in a micro-channel like the ones which can be found in a micro-combustor for instance. The reflection coefficient is indeed no more equal to zero in these cases. Moreover, as the radiation effect is neglectable in papers dealing with homogeneous reaction in small-ducts [Zhe – 2013] [Ghe – 2011] [Sch – 2015], the latter is not primarily set up in the micro-combustor CFD model. However, it could probably be added later to improve the model.

- The ***radiation*** model is not used in the micro-combustor simulations but could maybe be added later according to the experimental results.

Finally, it is shown in appendix n°21 and n°29 that the consideration of the temperature for the calculation of the dynamic viscosity is very important. The latter slightly increases the maximum flame temperature by about **3 %** but also redraws the shape of the flame making it more accurate and making the temperature profile closer to the experimental results.

- The consideration of the temperature using the ***Sutherland's law*** is used in the following simulations

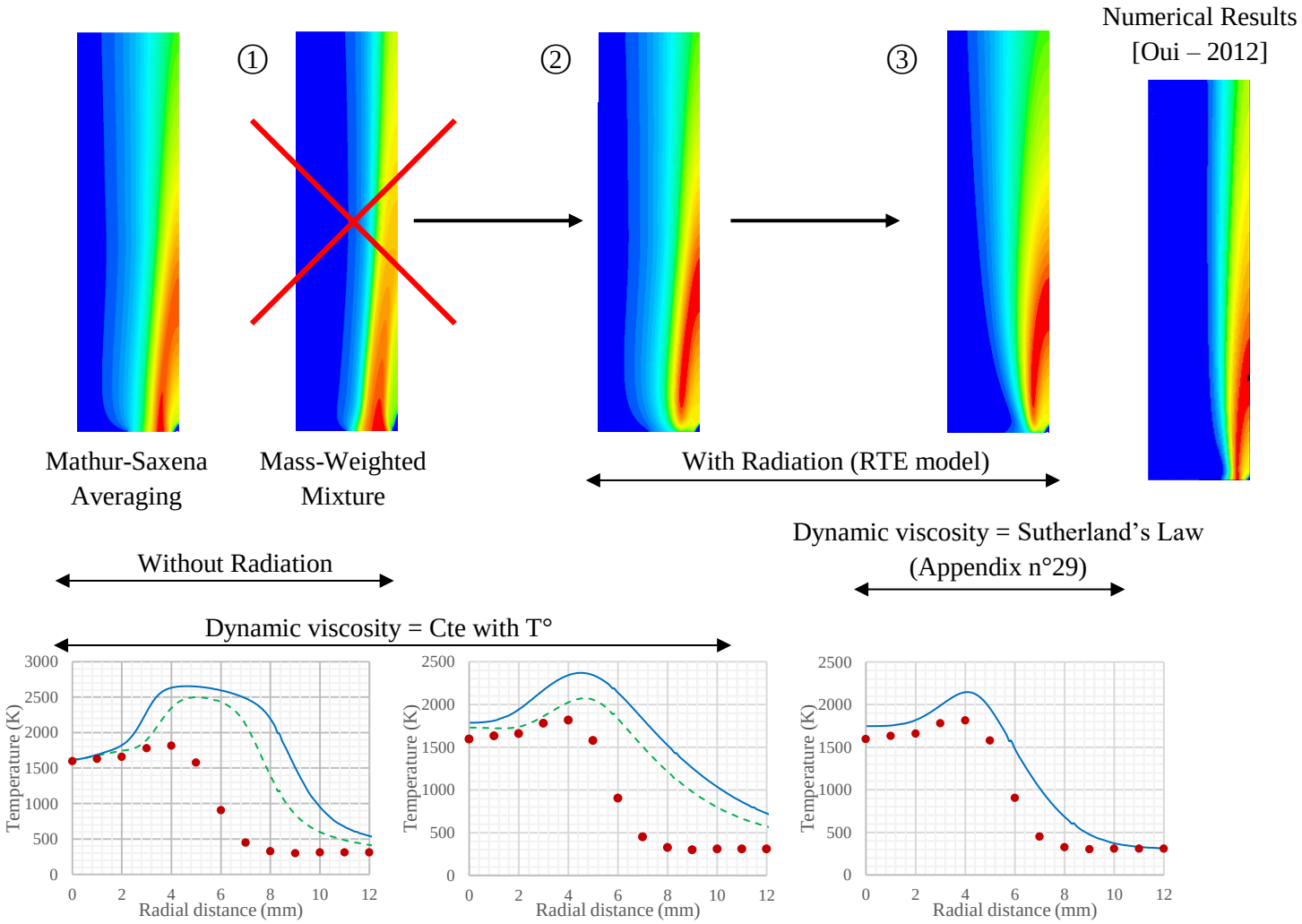

Figure 9: Enhancement of the numerical model for the validation of the homogeneous phase combustion reaction mechanism (Temperature profile)

The flame height

The flame height is defined by the height of the OH mole fraction profile whose figure is shown in appendix n°29. The numerical height of the OH mole fraction profile fits accurately the one got by Mrs. Ouimette in her Ph.D. thesis with approximately **66 mm**. The experimental value for the flame height is **68 mm** which gives a deviation of about **3 %**. The height for the CO, H_2 and O_2 numerical mole fraction profiles are slightly superior to the numerical results got by Mrs. Ouimette with a deviation of about 17 %, 32 % and 23 % respectively.

The temperature profile

The numerical results for the temperature profile are shown in appendix n°29. These latter overestimate the experimental results as showed in the table n°9. The difference between the numerical and the experimental results is maximum around the experimental value n°9 with a deviation between **93 %** (6mm) and **165 %** (38mm). The deviation is less important at the very beginning from the experimental value n°1 to the experimental value n°5 with a deviation between **5** and **20 %** approximately. At the very end, the deviation increases with the axial distance from **0 %** (6mm) to **70 %** (38mm) as the shape of the temperature profile grows faster in the simulations than in the reality. Nevertheless, the general shape of the temperature profile remains accurate and the main observed deviations can be linked to the wide spread of the temperature within the fluid domain. It seems that this phenomenon could be reduced by decreasing the dynamic viscosity value, but the analysis is not pursued further in this paper.

Table 9: Experimental / Numerical deviations for the temperature profile [Oui – 2012]

Experimental / Numerical deviations for the temperature profile [Oui – 2012]			
Radial distance	**Exp. point n°5 (Max)**	**Exp. point n°9 (Avg)**	**Exp. point n°13 (End)**
10 % - 6mm	2146 K	635 K	313 K
	1816 K	328 K	310 K
$\varepsilon_{10\%}$	**18.2 %**	**93.6 %**	**0.97 %**
20 % - 13mm	2197 K	1002 K	371 K
	1939 K	410 K	297 K
$\varepsilon_{20\%}$	**13,3 %**	**144.4 %**	**24.9 %**
40 % - 25mm	2102 K	1148 K	468 K
	1930 K	467 K	293 K
$\varepsilon_{40\%}$	**8.9 %**	**145.8 %**	**59.7 %**
60 % - 38mm	1878 K	1154 K	533 K
	1738 K	437 K	322 K
$\varepsilon_{60\%}$	**8.1 %**	**164.1 %**	**65.5 %**

The species mole fraction profile

The numerical results for the species mole fraction profiles are shown in appendix n°29. These latter fit very accurately the experimental values for the N_2, CO, O_2, H_2 and H_2O species regardless the axial position studied (6mm, 13mm, 25mm and 38mm). However, although the shape of the profile is preserved, a large deviation is observed between the numerical and the experimental values for the CO_2 mole fraction profile with experimental values more than twice greater than numerical results as showed in the table n°10. This deviation tends to decrease as the axial distance increases. In that respect, the CO_2 deviation is smaller for x=38mm than for x=6mm with experimental values which can reach ~ **+85%** / ~ **+350%** deviation with the respective numerical values.

Table 10: Deviation between numerical (-) and experimental (*) results for the CO_2 species [Oui – 2012]

Deviation between numerical (-) and experimental (*) results for the CO_2 species [Oui – 2012]

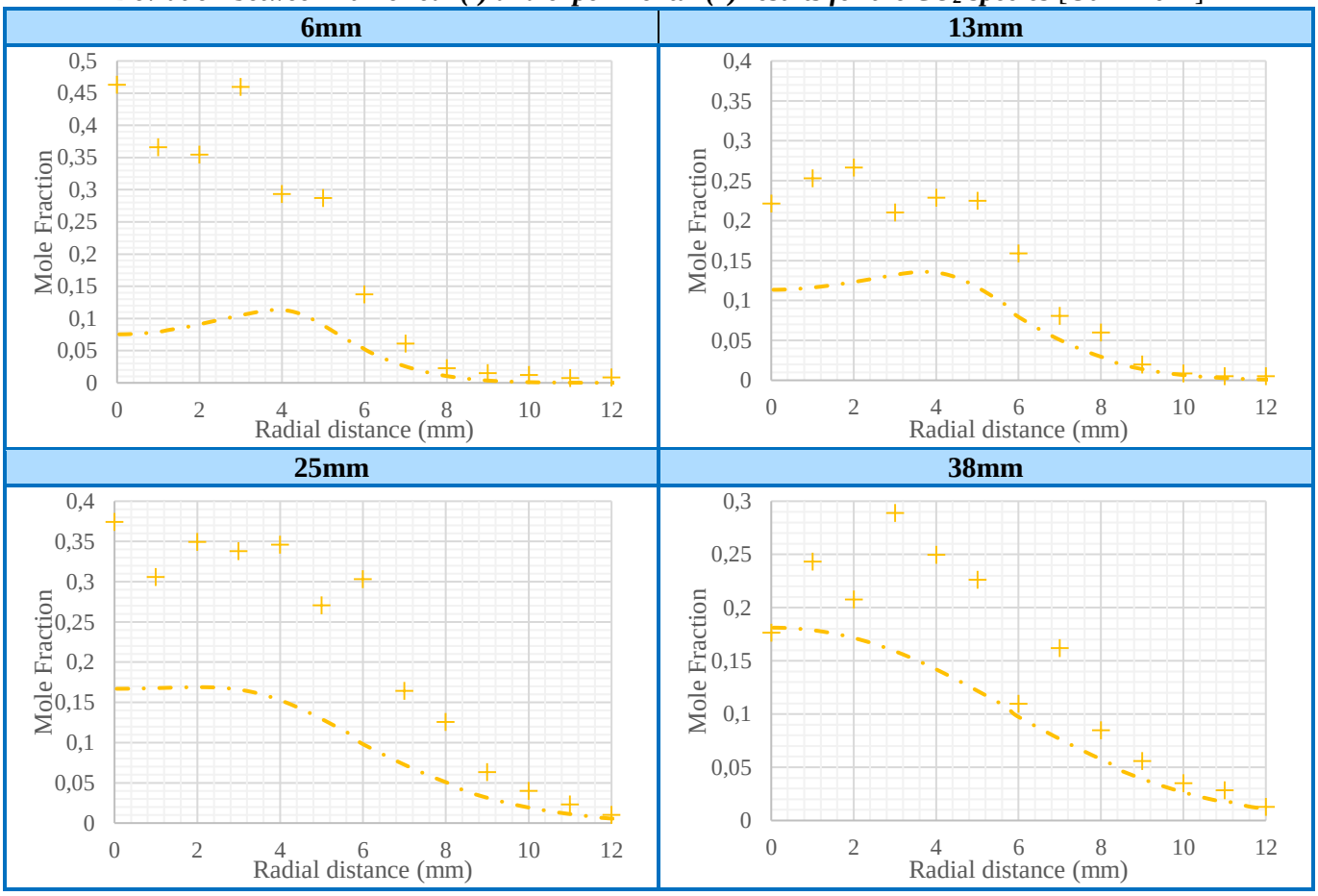

Conclusion

The axial flow velocity was perfectly validated running a cold flow simulation involving the associated H_2/CO/Air mixture as well as a fully-developed velocity profile calculated using the equation n°D.1 showed in appendix n°10. The validation of the ignited flow model was achieved focusing on three physical properties: the flame height, the temperature profile and the species mole fraction profiles. The flame height matches very accurately with the associated experimental value with a deviation of about 3 %. The species mole fraction profiles match pretty accurately with the associated experimental values regardless the axial position at the exception of the CO_2 whose the numerical concentration is far below the expected experimental concentration. Finally, although the numerical model overestimates greatly the temperature value especially for the average radial distances, the general shape of the temperature profile remains conserved. Furthermore, the deviation observed can be explained by a miscalculation of the mixture dynamic viscosity at high temperatures as the Sutherland's law is especially reliable for temperature between 300 K and 1200 K. By the way, it seems that the deviation decreases while the dynamic viscosity increases. The ideal gas hypothesis could also be a source of error.

5.2. Validation of the heterogeneous phase mechanism

The numerical model as well as the mesh were extracted from the Zheng et al. (2013) paper focused on the effect of hydrogen addition on the catalytic oxidation of carbon monoxide over platinum at power generation relevant temperatures [Zhe – 2013]. More generally, this study focused on the H_2/CO syngas mixture catalytic combustion within a narrow Pt-coated channel representative of the micro-combustor dimensions. In this paper, Zheng et al. (2013) developed a very simple 2D-numerical model in order to model their experiments and get numerical data for the species distribution as well as for the CO and H_2 conversion rate near the Pt-coated walls. In this part, the numerical values were attempted to be matched with the experimental results extracted from the Zheng et al. (2013) paper [Zhe – 2013]. The experimental cases n°3 and n°6 showed in the table n°11 were specifically investigated. The Zheng et al. (2013) computations were performed using a 2-D steady elliptic CFD code. The associated CFD software was not specified.

Table 11: Experimental conditions for the case n°3 and n°6 about the validation of the heterogeneous phase combustion mechanism [Zhe – 2013]

Experimental conditions of the case n°3 and n°6 [Zhe – 2013]					
	φ	$CO\ (\%\ Vol.)$	$H_2\ (\%\ Vol.)$	$T_{Inlet}\ (K)$	$U_{Inlet}\ (m.s^{-1})$
Case n°3	0.10	6.0	0.0	303	0.93
Case n°6	0.12	6.0	1.0	313	0.97

In order to allow relevant and reliable comparisons between the numerical results and those extracted from the Zheng et al. (2013) paper, the geometry design, the boundaries, the initial conditions, the mesh as well as the physical model and the associated hypothesis were reproduced as far as possible. Radiation was not considered in the following numerical model. The complete description of the model and underlying assumptions is displayed in appendix n°21.

The heterogeneous mechanism used by Zheng et al. (2013) was extracted from Deutschmann et al (2000) [Deu – 2000] whose mechanism is a reference for the modelling of the heterogeneous reaction of the $CH_4/H_2/CO$ mixture on Pt. Since the considered mixture does not include methane, the CH_4 reactions were removed as they were not relevant for the modelling of the heterogeneous reaction of H_2/CO on Pt. Several Arrhenius kinetic coefficients were also modified in order to take into account more recent paper [Koo – 2009]. Likewise, the HCOO(S) related reactions were added to the initial Deutschmann mechanism as their influence on the numerical results was shown to be significant in some specific cases. The homogeneous reactions were modelled using the Mantzaras et al. (2008) mechanism [Man – 2008] as it showed very good efficiency to model the homogeneous phase reaction in the part n°3. However, considering the very low equivalence ratio of the mixture ($0.1 < \varphi < 0.13$), the gas-phase chemistry is of negligible importance compared with the heterogeneous phase chemistry as the flammability limit of the mixture is not reached. In that respect, the choice of the latter appears to be less important [Zhe – 2013] [Che – 2017]. The results are considered convergent as soon as the residuals for each solved equation decrease under 1.10^{-4} which match with approximately 7500 iterations.

5.2.1. Geometry and boundary conditions

The geometry used is described in the figure n°10. The fluid domain is a simple 2D-rectangle 100 mm long per 7 mm wide. The Pt-coated channel used in the experiments was actually 200 mm long but since only the early oxidation of CO on the Platinum is of interest, the fluid domain was restricted to 100 mm long [Zhe – 2013].

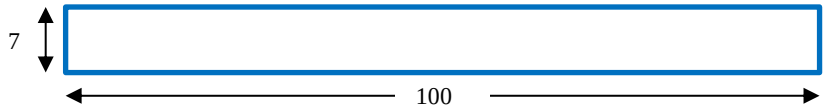

Figure 10: Geometry of the fluid domain for the validation of the heterogeneous phase combustion mechanism [Zhe – 2013]

The geometry represents a widely used experimental configuration for the study of micro-combustion in narrow channels as it is very simple and ease to implementation [Zhe – 2013] [Li – 2012] [Sch – 2015]. The boundaries of the previously described domain for the case n°6 are defined in the figure n°11. The upper and lower solid lines represent the two reactive walls. Their boundaries were chosen to "wall" with *temperature*, *impermeable*, and *no-slip* specification for the thermal, the species gradient as well as the shear stress specification respectively. The upper and lower wall temperature were constructed by fitting polynomials to thermocouple measurements. The left arrows represent a "Velocity Inlet" boundary condition whereas the right dashed line represents a "Pressure Outlet" boundary condition. The pressure, the temperature as well as the initial composition were chosen using the experimental values got for the case n°3 and n°6. The pressure of 5 bar and the walls temperature (600 K – 800 K) are relevant to describe the operating conditions of large and micro-turbine-based power generation devices [Zhe – 2013].

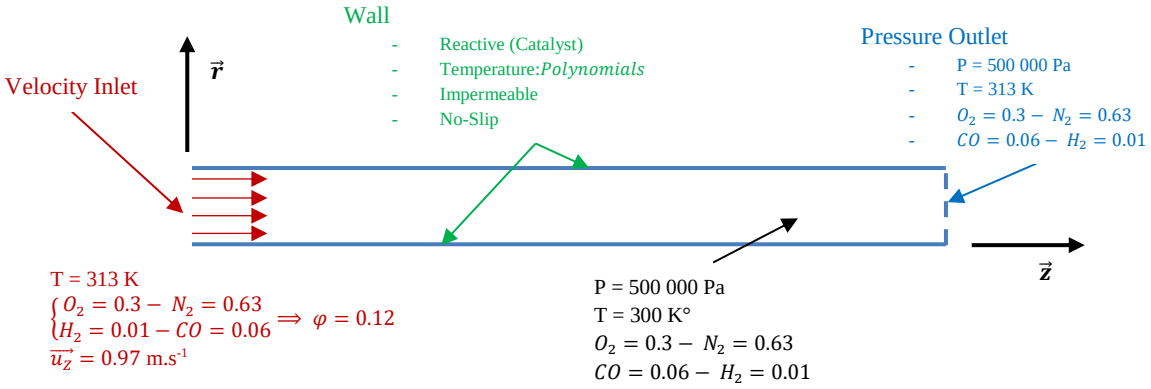

Figure 11: Boundary conditions of the fluid domain for the validation of the heterogeneous phase combustion mechanism Case n°6 - [Zhe – 2013]

5.2.2. Mesh

The mesh applied on the fluid domain is very simple and described on the figure n°12. The mesh refinement is realised by Zheng et al. (2013), therefore it is not developed there. The fluid domain is divided into 280*80 cells constantly distributed. In that respect, the size of an element is 0.357 mm long and 0.875 mm large. The cell size is constant on the whole fluid domain.

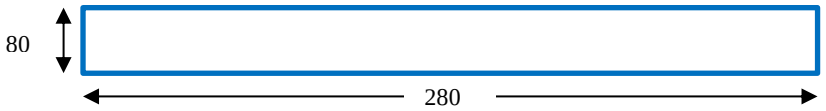

Figure 12: Mesh of the fluid domain for the validation of the heterogeneous phase combustion mechanism [Zhe – 2013]

5.2.3. Ignition method

Considering that the channel is initially filled with the reactive H_2/CO mixture in the appropriate proportion and at a pressure of 5 bar, the heterogeneous combustion reaction of the H_2/CO mixture on Pt is triggered due to the high temperature of the Pt-coated walls of the channel. The heterogeneous phase reaction starts instantaneously and evolves till reaching the steady state. The gas-phase contribution to syngas oxidation can be ignored in the range of operating conditions considered here [Zhe – 2013] [Che – 2017].

5.2.4. Results

The heterogeneous numerical validation was carried out in two steps. First, the experimental results for the case n°3 involving a $CO/O_2/N_2$ mixture were reproduced in order to find the appropriate set of parameters for the reactivity of CO on platinum. Then, the experimental results for the case n°6 involving a $CO/H_2/O_2/N_2$ mixture were reproduced reusing the previously defined set of parameters to validate definitely the selected heterogenous combustion reaction mechanism as well as the choice of the modified Arrhenius coefficient. The experimental measured transverse profiles of CO and H_2 mole fraction were got via Raman and OH-LIF measurements.

Case n°3: Heterogeneous reaction of a pure CO mixture

As a reminder, the experimental conditions of the case n°3 are described in the table n°11. The validation of the heterogeneous reaction of CO on platinum was done using the original modified heterogeneous mechanism of Zheng et al. (2013) [Zhe – 2013] as explained in the part n°3. The first numerical results got with such a mechanism were greatly overestimated the reactivity of CO on platinum leading to an inaccurate CO mole fraction profile for case n°3 and then for case n°6 with the H_2 species. To solve this problem, the decision was made to modify an Arrhenius coefficient of a critical step involving the CO species within the heterogeneous mechanism. In that respect, the pre-exponential Arrhenius coefficient in the step CO + PT(S) => CO(S) was decreased from 0.84 to 0.60 as showed in the figure n°13 using a dichotomy method briefly illustrated in the table n°12. The choice of the 0.6 value for the pre-exponential Arrhenius coefficient improved greatly the numerical results for the mole fraction profile of the CO and H_2 species.

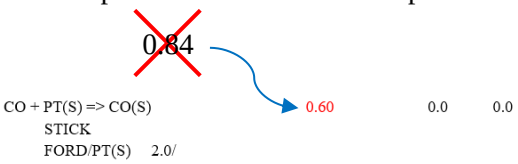

Figure 13: Modification of the pre-exponential Arrhenius coefficient in the CO+PT(S)=>CO(S) step

Table 12: Influence of the Arrhenius pre-exponential coefficient on the CO mole fraction profile (50mm)

Influence of the Arrhenius pre-exponential coefficient on the CO mole fraction profile (50mm)

0.45	0.55	0.60	0.84
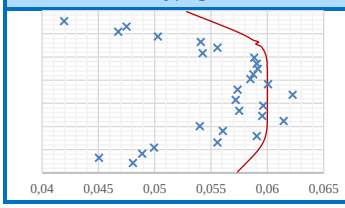	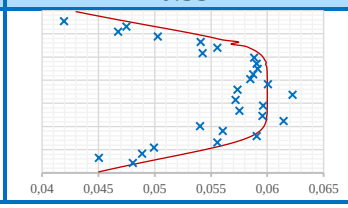	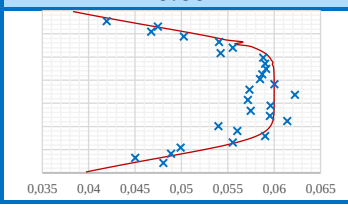	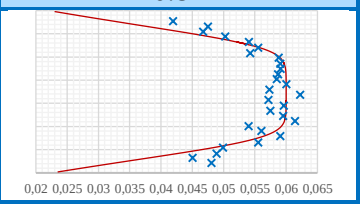

The appendix n°30 shows the numerical and the experimental superimposed results for the CO mole fraction at different axial position (8mm, 35mm and 50mm) for the case n°3. For each axial position, the numerical CO mole fraction values fit very accurately with the associated experimental results. The small resulting deviations are of the order of magnitude of the errors related to the experiments. This result is true in the middle of the channel where the heterogeneous reaction does not have any influence but also alongside the reactive Pt-coated walls where heterogeneous reactions were prominent.

Case n°6: Heterogeneous reaction of a CO / H_2 mixture

As a reminder, the experimental conditions of the case n°6 are described in the table n°11. The appendix n°31 shows the numerical and the experimental superimposed results for the CO and H_2 mole fraction at different axial position (8mm, 20mm and 35mm) for the case n°6. Similar to the previous case, the numerical results for the CO and the H_2 mole fraction profile fit very accurately with the associated experimental values. The small resulting deviations are of the order of magnitude of the errors related to the experiment. This result is especially valid at the 8mm and 20mm axial position. For the 50mm axial position, the numerical results seem to slightly overestimate the reactivity of H_2 and CO on platinum. The presence of unexplained small numerical instabilities for the 50mm axial position has also to be highlighted. Nevertheless, the numerical results for the CO and H_2 mole fraction profiles remain very accurate especially in the middle of the channel but also alongside the reactive walls where heterogeneous reactions are prominent. This general result is valid on a wide range of axial position. This study validates the choice of the Zheng et al. (2013) heterogeneous mechanism but highlights the importance of modifying an Arrhenius coefficient on a critical step to greatly enhance the accuracy.

Conclusion

The selected heterogeneous mechanism was extracted from the Zheng et al. (2013) paper and modified decreasing the pre-exponential Arrhenius coefficient in the step CO + PT(S) => CO(S) from 0.84 to 0.60. This small modification allowed the numerical CO and H_2 mole fraction profiles to fit very accurately with the associated experimental profiles extracted from the Zheng et al. paper (2013) whatever the axial distance considered. It can be noticed that for the case n°6, at the axial distance x=35 mm, the numerical H_2 mole fraction profile slightly overestimates the reactivity of the latter and thus, returns numerical H_2 mole fraction values smaller than the experimental ones. Some numerical imperfections can also be noticed.

5.3. Validation of the mechanism of the homogeneous reaction coupled with the heterogeneous reaction

The numerical model as well as the mesh were extracted from the Ghermay et al. (2011) paper [Ghe – 2011] as well as from the Schultze et al. (2015) paper [Sch – 2015] focused on the study of the hetero-/homogeneous combustion reaction of syngas mixture involving CO, H_2 as well as O_2 and N_2 over platinum at fuel-lean [Ghe – 2011] / fuel-rich [Sch – 2015] stoichiometries and pressures up to 5 bar [Ghe – 2011] / 14 bar [Sch – 2015]. These two studies took over the experimental apparatus as well as the model studied in the previous part n°5.2. In that respect, the dimensions as well as the 2D-numerical model of the narrow Pt-coated channel used in these papers were very similar to the previously described one. In this part, the numerical data were attempted to be match with the experimental and numerical results extracted from the Ghermay et al (2011) paper via the case n°8 and from the Schultze et al. (2015) paper via the case n°13. The experimental conditions related with these two cases are shown in the table n°13 and n°14. The case n°1 and n°3 as well as the case n°2 and n°4 from the Ghermay et al. (2011) and Schultze et al. (2015) respectively were also investigated regarding the shape of the flame only. The experimental conditions related with these cases are shown in appendix n°21. For both papers, computations were performed using a 2-D steady elliptic CFD code. The associated CFD software was not specified.

Table 13: Experimental conditions of the case n°8 for the validation of the homo-/heterogeneous phase coupled combustion mechanism with a fuel lean mixture [Ghe – 2011]

Experimental conditions of the case n°8 [Ghe – 2011] – (Fuel-lean)					
Case n°8	φ	$P\ (Bar)$	$r = H_2/CO$	$T_{Inlet}\ (K)$	$U_{Inlet}\ (m.s^{-1})$
	0.33	5	1:2	426	1.1
		$CO\ (\%\ Vol.)$	$H_2\ (\%\ Vol.)$	$O_2\ (\%\ Vol.)$	$N_2\ (\%\ Vol.)$
		0.078	0.039	0.177	0.706

Table 14: Experimental conditions of the case n°13 for the validation of the homo-/heterogeneous phase coupled combustion mechanism with a fuel-rich mixture [Sch – 2015]

Experimental conditions of the case n°13 [Sch – 2015] – (Fuel-rich)					
Case n°13	φ	$P\ (Bar)$	$r = H_2/CO$	$T_{Inlet}\ (K)$	$U_{Inlet}\ (m.s^{-1})$
	7	7	5:1	336	0.9
		$CO\ (\%\ Vol.)$	$H_2\ (\%\ Vol.)$	$O_2\ (\%\ Vol.)$	$N_2\ (\%\ Vol.)$
		0.1246	0.623	0.053	0.1994

As previously, in order to allow relevant and reliable comparison between the numerical results and those extracted from the Ghermay et al. (2011) and Schultze et al. (2015) papers, the geometry design, the boundaries, the initial conditions, the mesh as well as the physical model and the associated hypothesis were reproduced as far as possible. Radiation was not considered in the following numerical model. The heterogeneous mechanism used was identical to the one used in the part n°5.3 and was extracted from the Zheng et al. (2013) paper. The homogeneous reactions were modelled using the Mantzaras et al. (2008) mechanism [Man – 2008]. The results are considered convergent as soon as the residuals for each solved equation decrease under 1.10^{-4} which match with approximately 7500 iterations.

5.3.1. Geometry and boundary conditions

The geometry used is described in the figure n°14. The fluid domain is a simple 2D-rectangle 300 mm long per 7 mm wide. The depth of the channel which is 104 mm long is not represented there as a 2D model is used.

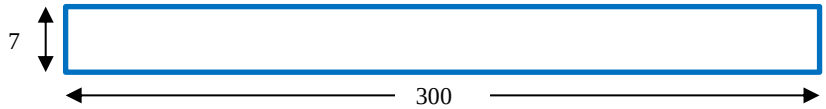

Figure 14: Geometry of the fluid domain for the validation of the homo-/heterogeneous phase coupled combustion mechanism [Ghe – 2011] [Sch – 2015]

The boundaries of the previously described domain are defined in the figure n°15. The upper and lower solid lines represent the two reactive walls. Their boundaries were chosen to "wall" with *temperature*, *impermeable*, and *no-slip* specification for the thermal, the species gradient as well as the shear stress specification respectively. The upper and lower walls temperature profiles were constructed by fitting polynomials to thermocouple measurements. The left arrows represent a "Velocity Inlet" boundary condition whereas the right dashed line represents a "Pressure Outlet" boundary condition. The pressure, the temperature as well as the initial composition were chosen using the experimental values got from the selected cases. The pressure between 1 and 14 bar and the walls temperature (750 K – 1250 K) are relevant to describe the operating conditions of a wide range of combustion driven power generation systems.

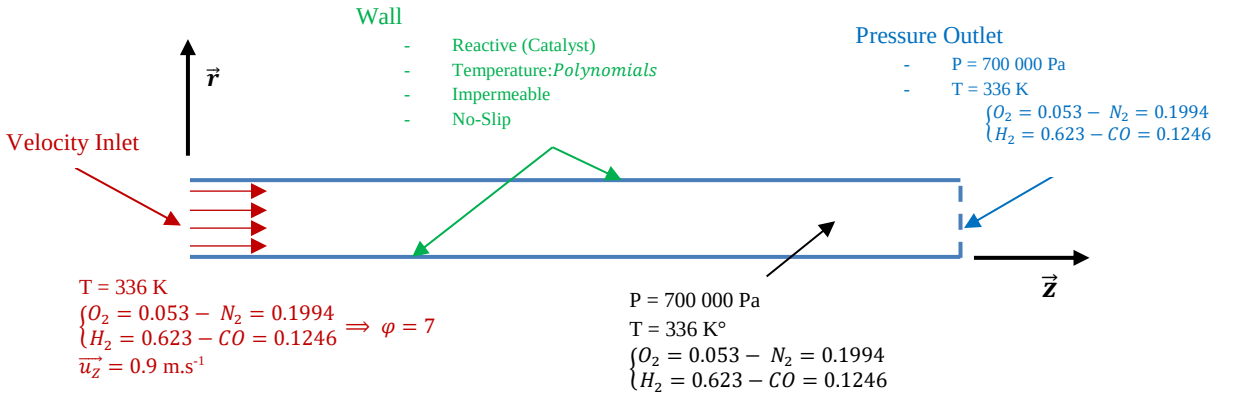

Figure 15: Boundary conditions of the fluid domain for the validation of the homo-/heterogeneous phase coupled combustion mechanism Case n°13 - [Sch – 2015]

5.3.2. Mesh

The mesh applied on the fluid domain is very simple and described on the figure n°16. The mesh refinement is realised by Ghermay et al (2011) / Schultze et al. (2015), therefore it is not developed here. The fluid domain is divided into 480*100 cells constantly distributed. In that respect, the size of an element is 0.625 mm long and 0.8 mm large. The cell size is constant on the whole fluid domain.

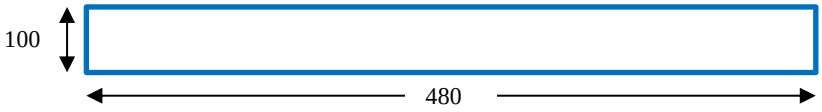

Figure 16: Mesh of the fluid domain for the validation of the homo-/heterogeneous phase coupled combustion mechanism [Ghe – 2011] [Sch – 2015]

5.3.3. Ignition method

The channel was initially filled with the reactive H_2/CO mixture in the appropriate proportion, temperature and pressure. In that respect, the heterogeneous combustion reaction of the H_2/CO mixture on Pt and the homogeneous combustion reaction were triggered thanks to the high walls temperature set up via the wall temperature boundary condition [Ghe – 2011] [Sch – 2015].

5.3.4. Results

The experimental mole fraction profiles for the H_2, CO, O_2, CO_2 and H_2O species got via Raman-measurements were reproduced numerically. The associated flame height got via OH-LIF measurement was also tried to be found to definitely validate the use of the Mantzaras et al. (2008) and Zheng et al. (2013) mechanisms as well as the use of the previously quoted model. The cases n°2 and n°4 as well as the cases n°1 and n°3 for the fuel-rich / fuel-lean condition respectively were investigated in appendix n°32 and n°33.

Case n°8: CO/H₂/Air fuel-lean mixture

The experimental results were extracted from the Ghermay et al. (2011) paper [Ghe – 2011].

Table 15: Experimental (8A) and numerical (8B) OH mole fraction for the case n°8 [Ghe - 2011]

***Experimental (8A) and numerical (8B) OH mole fraction for the case n°8* [Ghe – 2011]**

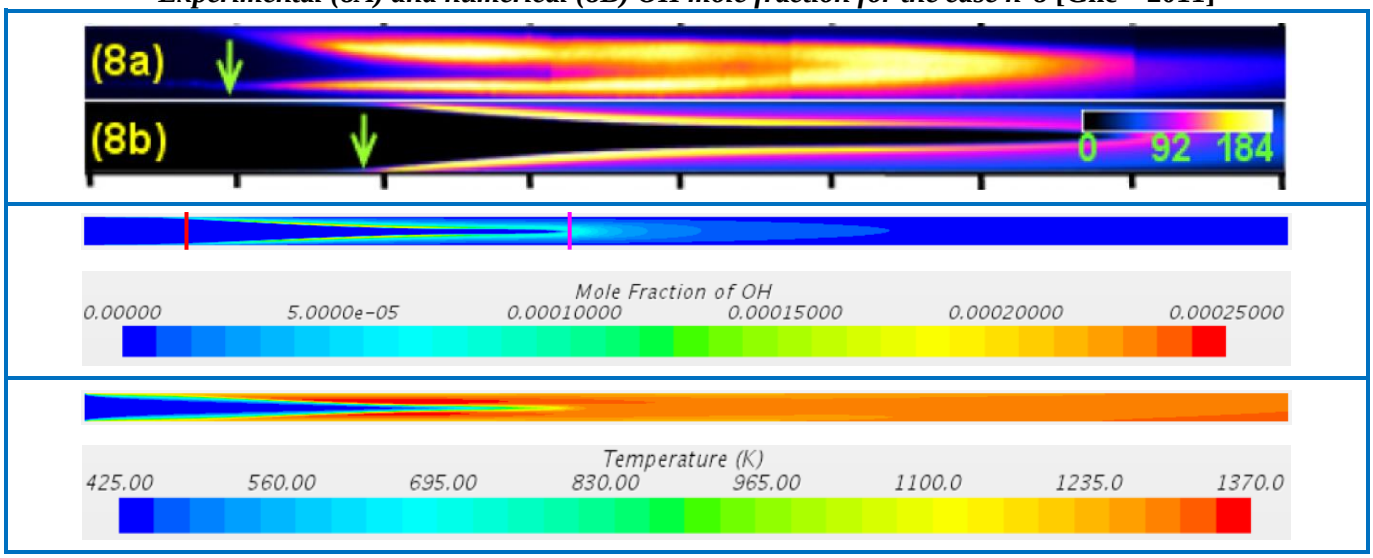

The table n°15 presents the numerical OH mole fraction and temperature associated with the experimental OH-LIF measurements picture on the figure (8A) for the case n°8. Similar tables for the case n°1 and n°3 are shown in appendix n°32. For each fuel-lean case, the flame height is smaller than the experimental one. In the case n°8 showed in the table n°15, the experimental flame height is about **33 %** higher than the numerical one. For the case n°1 and n°3, the experimental flame height is respectively about **1.5 %** lower and **45 %** higher than the numerical one. However, the numerical position of the flame ignition for each of the three cases is pretty accurate as the deviation between experimental and numerical position is only **13mm**, **7.5mm** and **12mm** respectively which matches with **4.3 %**, **2.5 %** and **4 %** of the whole channel length. These results are summed up in the table n°16.

Table 16: Comparison between experimental and numerical position of the flame in the case of a fuel lean-mixture

	Flame height (mm)	$\frac{FlameHeight_{Exp}}{FlameHeight_{Num}}$	Flame ignition distance (mm)	$\frac{FlameIgnDis_{Exp}}{FlameIgnDis_{Num}}$
Case n°8 – Experimental Results	182	**1.49**	37	**1.54**
Case n°8 – Numerical Results	122		24	
Case n°1 – Experimental Results	244	**0.99**	15	**0.67**
Case n°1 – Numerical Results	247.5		22.5	
Case n°3 – Experimental Results	141	**1.83**	28	**1.75**
Case n°3 – Numerical Results	77		16	

The numerical CO, CO_2, H_2 and H_2O mole fraction profiles for the case n°8 were taken at 10mm, 25mm and 40mm from the channel entrance. They are shown in appendix n°32. These latter fit accurately the experimental mole fraction profiles in particular at the very beginning (10mm – 25mm) and in the middle of the micro-channel. The deviations observed are of the order of magnitude of measurement uncertainties. As going further down the channel (40mm), the homogeneous phase combustion begins to impact the species mole fraction profiles and therefore, the numerical results for the studied species slightly underestimate / overestimate the mole fraction of the consumed / created species. This result is due to the fact that for the case n°8, the flame ignition position appears slightly sooner in the numerical model than in the experiment.

Case n°13: CO/H_2/Air fuel-rich mixture

The experimental results were extracted from the Schultze et al. (2011) paper [Sch – 2015].

Table 17: Experimental (13A) and numerical (13B) O_2 mole fraction for the case n°13 [Sch - 2015]

***Experimental (13A) and numerical (13B) O_2 mole fraction for the case n°13* [Sch – 2015]**

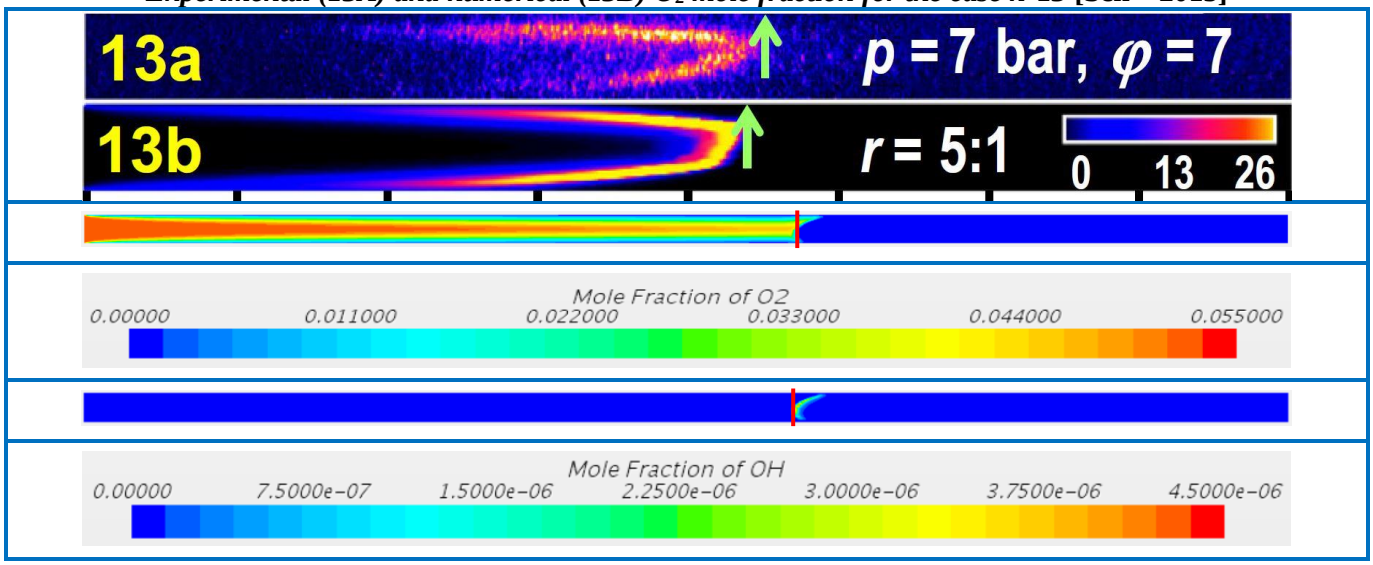

The table n°17 presents the numerical O_2 mole fraction and the temperature profile associated with the experimental hot O_2-LIF measurements picture on the figure (13A) for the case n°13. Similar tables for the case n°2 and n°4 are shown in appendix n°33. For each fuel-rich case, the flame position is approximately the same than the experimental one. In the case n°13 showed in the table n°17, the experimental flame height is about **6 %** lower than the numerical one. For the case n°2 and n°4, the experimental flame position is respectively about **19mm** lower and **3mm** higher than the numerical one which matches with **6.3 %** and **1 %** of the whole channel length respectively. These results are summed up in the table n°18.

Table 18: Comparison between experimental and numerical position of the flame in the case of a fuel rich-mixture

	Flame height (mm)	Flame ignition distance (mm)
Case n°13 – Experimental Results	169	***
Case n°13 – Numerical Results	178	***
Case n°2 – Experimental Results	***	124
Case n°2 – Numerical Results	***	143
Case n°4 – Experimental Results	***	131
Case n°4 – Numerical Results	***	128

The numerical O_2, CO, H_2, CO_2, and H_2O mole fraction profiles for the case n°13 were taken at 20mm from the channel entrance. They are shown in appendix n°33. The O_2 numerical mole fraction fits perfectly the experimental results while the CO and the H_2 numerical mole fraction slightly underestimates / overestimates the reactivity of the associated species. This leads to inaccurate mole fraction for the CO species especially, alongside the reactive platinum walls where the heterogeneous reaction takes place. Similar numerical results are observed for the H_2O and the CO_2 species which are respectively slightly overestimated / underestimated alongside the platinum walls.

Conclusion

The experimental flame height was reproduced fairly accurately by the numerical model for fuel-rich mixtures as showed by the case n°2, n°4 and n°13 in appendix n°33. The latter was less accurate for fuel-lean mixtures where deviations can reach 45 % as showed by the case n°1, n°3 and n°8 in appendix n°32. Moreover, the numerical species mole fraction profiles fitted pretty accurately the experimental mole fraction ones for fuel-lean mixtures. The observed deviations were of the order of magnitude of measurement uncertainties (Case n°1, n°3 and n°8 for fuel-lean mixtures [Ghe – 2011]). However, there were small deviations between the numerical and the experimental CO and H_2 mole fraction profiles for fuel-rich mixtures especially (Case n°13 [Sch – 2015]), alongside the reactive walls.

6. The micro-combustor numerical model

The design of a reliable numerical model for the micro-combustor is one of the main objectives of this project. Preliminary validation studies presented in the part n°5.1, n°5.2 and n°5.3 allowed to validate the previously selected homogeneous and heterogeneous combustion reaction mechanisms as well as to define a numerical model and its associated set of parameters. In that respect, the homogeneous and the heterogeneous combustion reaction mechanisms applied to the micro-combustor model are those extracted from the Mantzaras et al. (2008) paper [Man – 2008] and from the Zheng et al. (2013) paper [Zhe – 2013] respectively. The efficiency and the reliability of both mechanisms were demonstrated previously. In the following studies, the results are considered convergent as soon as the residuals for each solved equation decrease under 1.10^{-4} which match with approximately 2000-20000 iterations depending of the mesh refinement.

6.1. Geometry and boundary conditions

The numerical model of the micro-combustor was built considering the dimensions of the secondly designed device (V2) whose blueprints are available in appendix n°12-13-14-15-16-17-18-19 and 20. The geometry of the fluid domain is described in the figure n°17. The red dotted lines represent the gases inlets whereas the blue dashed lines represent the flue gases outlets. The green full lines inside the fluid domain represent the reactive platinum plate on which the heterogeneous combustion reactions take place. Although the fluid domain has an axis of symmetry, it is not relevant to reduce the fluid domain using the "symmetry" boundary condition since the micro-combustor is expected to receive inlet gases of different concentration depending on whether the upper or the lower channel is considered. Furthermore, as the two channels are interacting with each other via the hole in the platinum plate, what happens in one influences the other and vice versa, hence the importance of keeping the whole fluid domain.

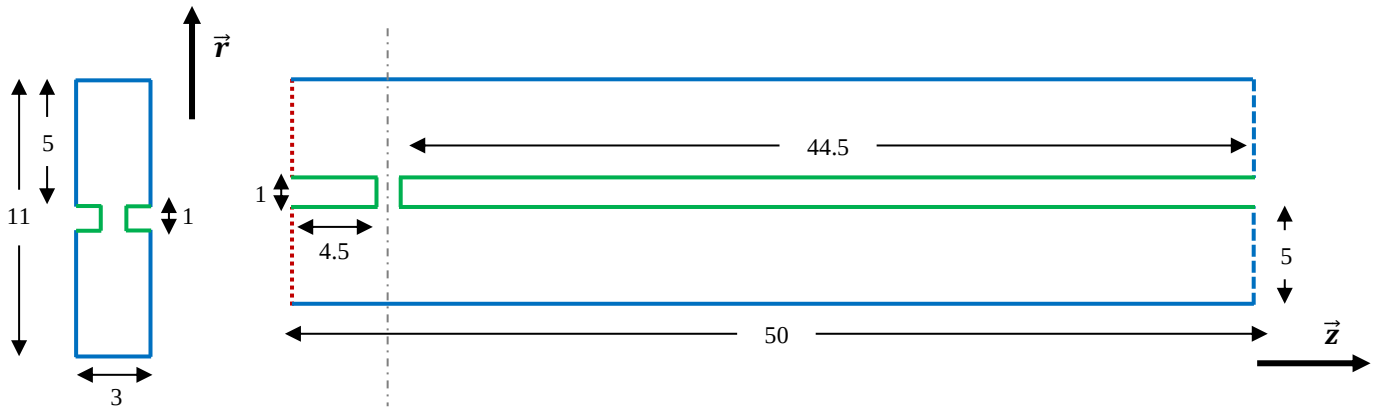

Figure 17: Geometry of the fluid domain for the numerical model of the micro-combustor V2

The fluid domain is 50 mm long, 11 mm high and 3 mm width which matches with the length and the width of the platinum plate. The 3D-fluid domain was then converted into a 2D-fluid domain to save computing time while performing some simple parametric studies. However, it should be noted that the hole on the platinum plate has small dimensions compared to the width of the platinum plate. Therefore, its influence on the width of the 3D model is probably non neglectable. In that respect, the 2D model returns pretty accurately the combustion process as well as the associated scalar values in the middle of the micro-combustor but under no circumstances may it be used to get results about the sides of the micro-combustor.

The boundaries of the fluid domain defined previously are described in the figure n°18. The red dotted line boundaries were chosen to "Velocity Inlet" with an inlet temperature of 300 K, a flow

velocity of 5 m.s^{-1} as well as an equivalence ratio of one with air as oxidizer ($X_{H_2} = 0.148$, $X_{CO} = 0.148$, $X_{O_2} = 0.148$, $X_{N_2} = 0.556$). Then, the blue dashed line boundaries were chosen to "Pressure Outlet" with a pressure, a temperature and a gas composition which matched with the standard atmospheric conditions (101325 Pa, 300 K, $X_{O_2} = 0.21$ / $X_{N_2} = 0.79$). Finally, the boundary of the micro-combustor walls represented by green and blue full lines was chosen to "Wall" with the *adiabatic*, *impermeable* and *no-slip* specifications for the thermal, the species gradient and the shear stress specification respectively.

The initial conditions within the domain match with the steady state of the cold flow without any combustion reactions:

- P = 101325 Pa
- T = 300 K
- Molar fraction = $X_{H_2} = 0.148$, $X_{CO} = 0.148$, $X_{O_2} = 0.148$, $X_{N_2} = 0.556$

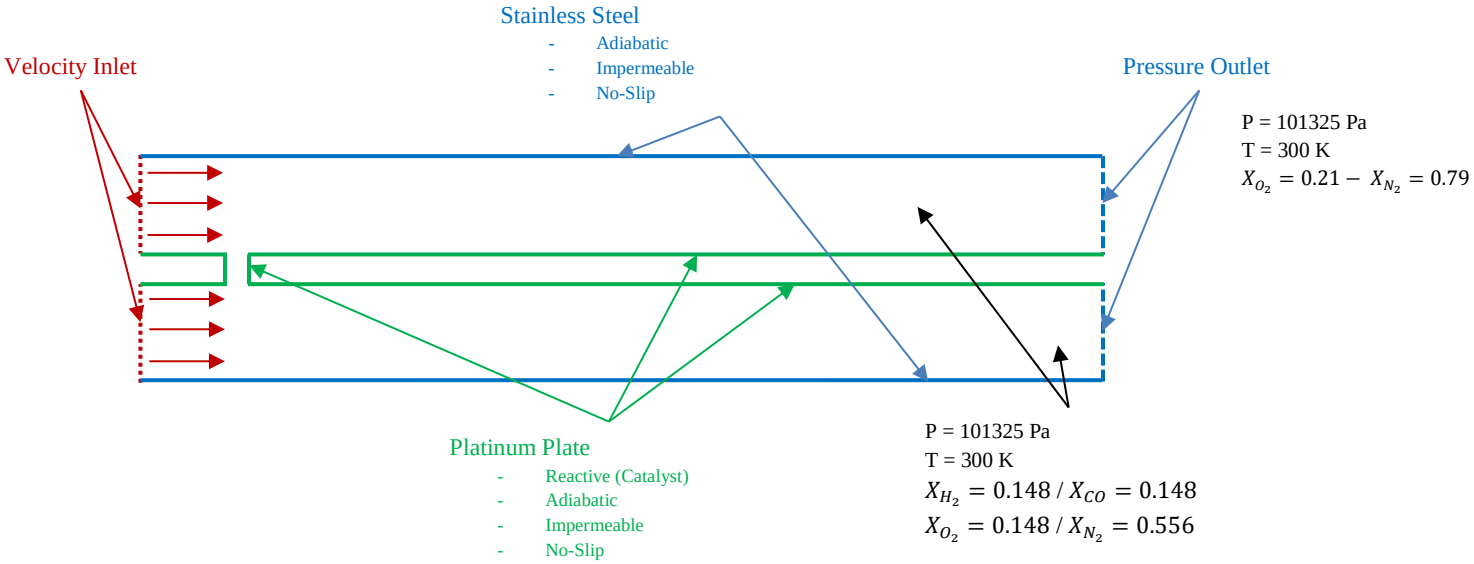

Figure 18: Boundary conditions of the fluid domain for the numerical model of the micro-combustor V2

6.2. Ignition method

The combustion process within the micro-combustor numerical model was triggered using the "ignitors" option. A temperature of 1500 K is applied to the whole model as a "pulse". It is triggered at the 20th iteration and remains active till the 40th iteration. The ignition is instantaneous, and the combustion is then auto-sustained by the elevate temperature, the presence of active radicals as well as the heterogeneous phase reaction once the ignitor turns off.

6.3. Mesh convergence

The objective of the mesh convergence is to find a compromise between computing time and accuracy of the numerical results. The basics of the mesh convergence method are very simple. Starting from a coarse mesh, the latter is progressively refined until the results no longer vary with a reduction in cell size. Usually, it is considered that the convergence is reached when for a new division of the mesh size, the results do not vary more than 1.0 %. In our case, different mesh sizes were tested and compared. Then, after processing of the results, a final refined mesh was designed combining the previously tested meshes taking into account their accuracy and the associated computing time. The different mesh sizes and characteristics used are showed in the figure n°19 as well as in the table n°19.

Numerical values were extracted at an axial distance of 2, 5 and 8mm from the inlet of the micro-combustor as well as in the middle of a channel as showed in the figure n°21 and n°22. The mesh n°12 showed in the table n°19 is a highly refined mesh which is considered as the reference with converged numerical values.

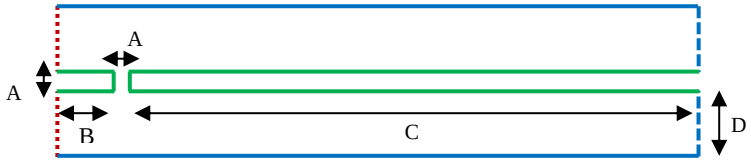

Figure 19: Number of cells in the micro-combustor model

Table 19: Synthesis of the mesh characteristics

Synthesis of the mesh characteristics

	A	B	C	D	Total		A	B	C	D	Total
Mesh n°1	2	9	89	10	2004	**Mesh n°6**	12	54	534	60	72144
Mesh n°2	4	18	178	20	8016	**Mesh n°7**	14	63	623	70	98196
Mesh n°3	6	27	267	30	18036	**Mesh n°8**	16	72	712	80	128256
Mesh n°4	8	36	356	40	32064	**Mesh n°9**	18	81	801	90	162324
Mesh n°5	10	45	445	50	50100	**Mesh n°10**	20	90	890	100	200400
						Mesh n°12	24	108	1068	120	288576

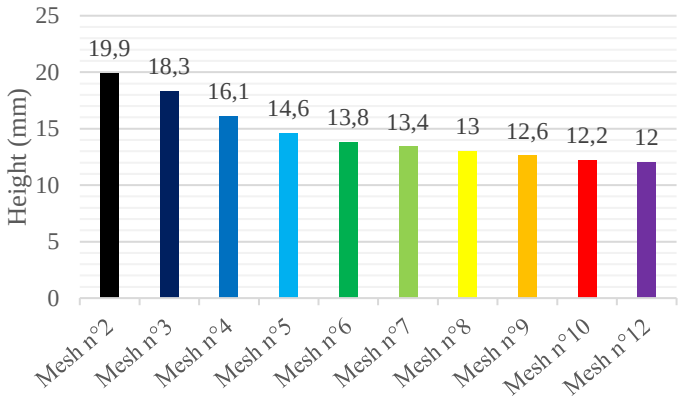

Figure 20: Flame height for each different mesh

6.3.1. Mesh convergence on the flame height

The figure n°20 shows the height of the flame for each mesh size. The mesh n°1 is too coarse to be able to identify a relevant flame height, therefore it is not showed here. The flame height is defined using the OH mole fraction as explained in the part n°6.3.3.

The flame height can be considered as converged from mesh n°10 as the height difference between the mesh n°10 and the reference mesh n°12 is only of 0.2mm with a deviation of about **1.6%.**

Table 20: Flame height comparison and deviation for each different mesh

Flame height comparison

	Mesh n°2	Mesh n°3	Mesh n°4	Mesh n°5	Mesh n°6	Mesh n°7	Mesh n°8	Mesh n°9	Mesh n°10	Mesh n°12
Flame height (mm)	19.9	18.3	16.1	14.6	13.8	13.4	13.0	12.6	12.2	12.0
Deviation (%)	***	-8.0	-12.0	-9.3	-5.5	-2.9	-3.0	-3.1	-3.2	-1.6

6.3.2. Mesh convergence on the near hole axial profile

The axial positions are located at 2mm, 5mm and 8mm, near the platinum hole which is the area of interest as showed on the figure n°21. The OH mole fraction, the temperature as well as the flow velocity profiles are studied for each axial location. The previously quoted profiles for each different mesh are compared and showed in appendix n°35.

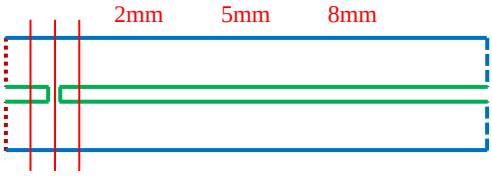

Figure 21: Axial position for the measurement of temperature, OH mole fraction and velocity profiles

Whether for the OH mole fraction, the temperature or the flow velocity, the mesh n°3, n°4, n°5 and n°6 do not return very accurate values and profiles in particular at the walls of the micro-combustor (0.00mm and 7.00mm). Therefore, this four-coarse meshes are discarded to represent the combustion process in the area of interest, where the flame hanger, in the vicinity of the hole. Finally, it appears that only the mesh n°10 returns accurate converged values in this area, whether for the temperature, the OH mole fraction or the velocity profile. This observation is particularly true for the 2mm and 5mm axial position but as the distance with the hole increases, the deviation between the previously defined mesh gradually decreases.

6.3.3. Mesh convergence on the radial profile

The studied radial position is located at 2.5mm in the lower channel so that the radial profile intersects with the end of the flame as showed on the figure n°22. The radial OH mole fraction as well as the temperature profiles are studied for each different mesh. The peak of OH mole fraction allows to define the height of the flame. The meshes n°3, n°4, n°5 and n°6 were previously discarded as they did not return accurate profiles near the walls of the micro-combustor.

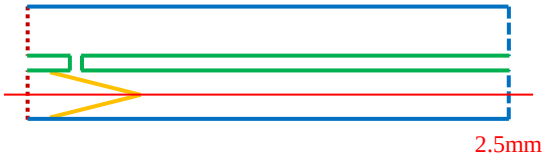

Figure 22: Radial position for the measurement of temperature and OH mole fraction profiles

- ***The temperature / OH mole fraction profile***

The radial temperature as well as the OH mole fraction profiles and deviations for each different mesh at some specific locations are showed in appendix n°35. From 0mm to 20mm, in the vicinity of the hole, the mesh convergence is reached for the mesh n°10 as the deviation for the temperature and the OH mole fraction profile compared to the mesh n°9, is of **0.5 %** in each case. A very big deviation can be noted at 5mm - 10mm for the temperature / OH mole fraction profile but the latter seems to come from a numerical error as showed in the associated figure in appendix n°35. From 20mm to 30mm, the meshes n°8, n°9 and n°10 can be considered as converged as the deviation between the mesh n°8 and the mesh n°10 does not exceed **1.0 % / 2.0 %** for the temperature profile and the OH mole fraction profile respectively. From 30mm to 50mm, the meshes n°5, n°6, n°7, n°8, n°9 and n°10 all return the converged value for the temperature / OH mole fraction and the associated deviations do not exceed **1.0 % / 2.0 %** (**0.1% / 0.5 %** if we only considered the meshes n°7, n°8, n°9 and n°10).
To conclude, the characteristics of the mesh n°10 should be used at least till 20mm, in the vicinity of the hole. Then the number of cells can be decreased to reach the characteristics of the mesh n°8 till 30mm. Finally, the number of cells can still be reduced to reach the characteristics of the mesh n°5 till 50mm.

6.3.4. Design of the final mesh

Two different meshes were designed and compared using the analysis of the results extracted during the mesh convergence detailed in parts n°6.3.1, n°6.3.2 and n°6.3.3. These latter are described in the table n°21. Their associated axial and radial temperature, OH mole fraction and velocity profiles are showed in appendix n°36. The mesh V1 is defined by the number of cells and has the radial characteristics of the meshes n°10, n°8, n°6 and n°4 between 0-20, 20-30, 30-40, 40-50mm respectively. The number of cells in the width of a channel is 100, no matter the area considered. The mesh V2 is defined by the size of a cell and has the characteristics of the meshes n°10, n°5 and n°2.5 between 0-20, 20-40 and 40-50mm respectively. Both mesh types are very close in terms of mesh size and design. However, the V1 mesh type has 152 400 cells while the V2 mesh has 103 148 cells which greatly influence the time calculation as showed thereafter.

Table 21 : Converged mesh V1 (on the left) and converged mesh V2 (on the right)

Converged mesh V1 (on the left) and converged mesh V2 (on the right)	
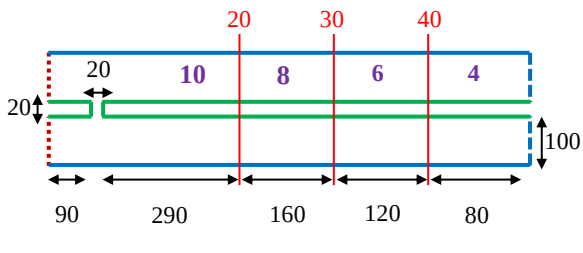	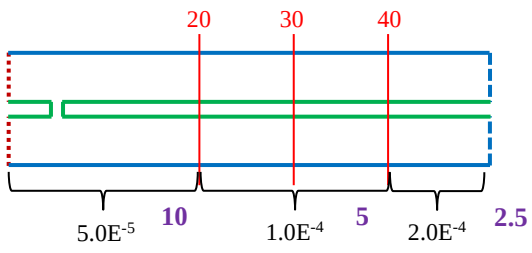
Number of cells	***Size of cells (m)***
152 400 cells	**103 148 cells**

The appendix n°36 shows that there are almost no deviations between the mesh n°10 and the converged meshes V1 and V2 showed in the table n°21, for the axial positions 2mm, 5mm and 8mm in the vicinity of the platinum hole. This shows that the mesh for the model V1 and V2 is sufficiently refined to describe the combustion process in the area of interest near the hole, where the flame hangs. The same observation can be made between 20mm and 50mm where the mesh gets coarser. As showed in the figure n°23, the V1 model numerical results fit perfectly with the numerical results get with the mesh n°10 whether for the OH mole fraction or the temperature profiles while the V2 model slightly overestimates the OH mole fraction profile.

Finally, considering the great accuracy of the results in both cases, the final selected mesh is the model V2 due to its convergence more than twice faster than the V1 model convergence and its great accuracy.

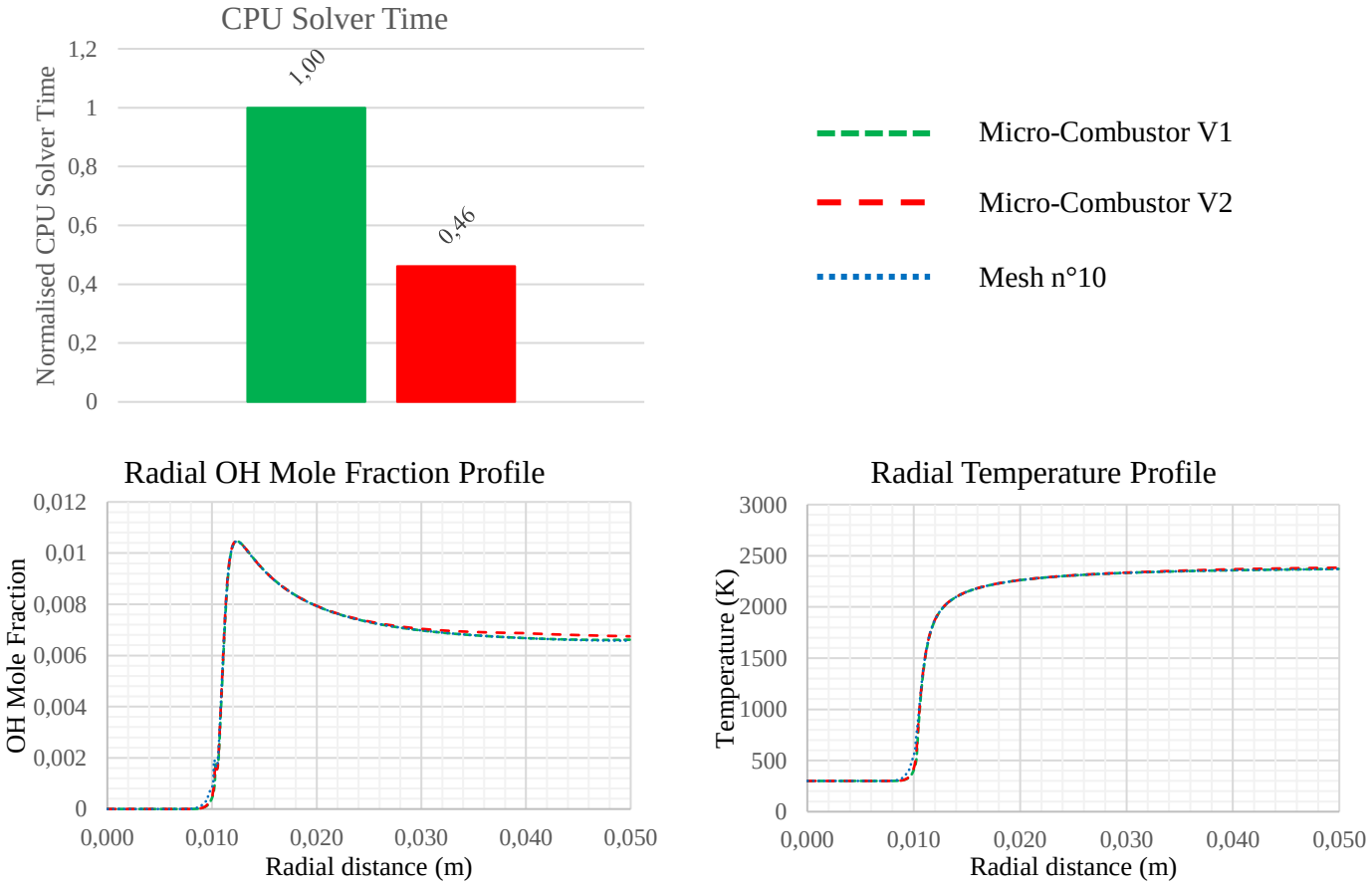

Figure 23: CPU solver time and radial OH mole fraction / temperature profiles for the mesh V1 and V2

7. Conclusion

7.1. Scientific conclusion

As part of my second year of a Master of mechanical and pyrotechnic engineering at ENSTA Bretagne, I carried out my final year project between the 26th of March 2018 and the 17th of August 2018 (21 weeks) within the combustion and propulsion laboratory of the Aeronautics and astronautics department of NCKU in Tainan, Taiwan. During this five-month internship, I was tasked with developing, measuring as well as simulating a simple micro-combustor embedding a platinum plate in the middle for a bio-syngas combustion driven thermophotovoltaic power system. This research project fell as part of a larger project bringing together several universities and laboratories. The final objective was the development of an optimised TPV device which could provide power for an industrial application once assembled in series. The combustion laboratory of NCKU oversaw the development of the micro-combustor. The whole research project took place under the supervision of Pr. Yueh-Heng Li (李約亨). I worked in collaboration with two master students **Chien-Chun Kao** (高建鈞) and **Davy Sawadogo** whose master thesis topic was very close to my final year internship one.

A reliable and efficient micro-combustor CFD model was designed using the StarCCM+® CFD software. This model was built using the "Complex chemistry" combustion model which was appropriate to simulate precisely combustion reactions using detailed kinetic mechanisms. The $H_2/CO/O_2$ reaction mechanisms used was selected via preliminary bibliographic researches and the building of the micro-combustor model took place in three steps. Firstly, the homogeneous as well as the heterogeneous phase mechanisms were validated independently reproducing the experimental data got by Mrs. Ouimette in her Ph.D. Thesis as well as by Zheng et al. (2013) respectively. Then, a final validation involving both homogeneous phase and heterogeneous phase mechanisms was performed reproducing the experimental data got by Ghermay et al. (2011) and Schultze et al. (2015) for fuel-lean and fuel-rich mixtures respectively. Finally, a CFD model as well as the associated mesh convergence reproducing the micro-combustor was made based on the previously built simulation parameters.

In order to validate the numerical results and study the influence of the input parameters on the combustion process, a campaign of experiments should had been made varying the inlet flow rate, the inlet gas composition as well as the position of the hole. Unfortunately, the first design of the micro-combustor involving two quartz plates for the observation of the combustion process was not functional because of a sealing issue at the junction between the quartz plates and the main body of the micro-combustor. This issue was firstly unsuccessfully solved using high resistant temperature carbon graphite seals and then using a high temperature resistant copper-based silicone to replace Teflon® seals. Finally, a new micro-combustor involving a single quartz plate, whose structure was mainly inspired from the first one was designed to replace the previous one and fix the issue. The main body of the latter was separated in two parts for machining reasons while a slot was added to provide the Teflon® ring, used to seal the junction between the quartz plate and the main body, to be in contact with the flame. The two quartz plates were replaced by a single one to improve the visibility of the combustion process while providing a slot to keep the platinum plate upright. This choice was also aimed to prevent leaks by removing several interfaces between the quartz plate and the main body. A small campaign of experiments should had been run at the end of the internship to determine the range of application of the new micro-combustor regarding the inlet gas composition for a preheating of 500 K and considering that the Air represented half of the inlet gases. However, although everything was set-up to pursue the experiments, the latter was not conducted by lack of time.

During this internship, I contributed to launch a new project regarding the design, the use and the simulation of a new rectangular shaped micro-combustor for a bio-syngas combustion driven thermophotovoltaic power system. In that respect, I built a reliable numerical model whose mechanism as well as parameters were validated reproducing experimental results extracted from literature for many different cases. I also designed an enhanced version of the micro-combustor fixing leak issues and improving the visibility of the combustion process. However, this is a longstanding project which needs to be continued. In that respect, it could be interesting, first and foremost to conduct a campaign of experiments and fully determine the range of application of the micro-combustor varying the inlet flow rate, the inlet gas composition and the position of the hole on the platinum plate. This campaign of experiments coupled with a numerical study should allow to determine the operating point where the combustion process is the most effective and thus focus the study on a more precise area of interest. Then, although the use of platinum in the micro-combustor is compulsory to improve the combustion reaction and so on the micro-combustor efficiency, the latter is a very expensive metal with a price close to two thirds of that of gold. In that respect, it could be interesting to conduct another study to try to reduce the volume of platinum while conserving the efficiency of the micro-combustor and thus decrease the cost-effectiveness of the device. Finally, in view of the current ecological and environmental concerns, it could also be relevant to add the NOx related formation reactions to the global mechanism to conduct a numerical study about the pollutant emissions. This study could be completed and validated by a campaign of experiments and would allow to find an operating point where the ratio of pollutant emissions to efficiency is minimal.

7.2. Personal conclusion

First of all, this final year project was an opportunity to discover the functioning of a university research laboratory which was a pretty unknown structure on both the functioning and the work organisation and thus to define more precisely my professional and career project. Bolstered by this experience, I reiterate my willingness to work in a multi tasks job involving both computing, simulations and experiments as well as representation and management tasks to keep the technical but also the social aspect of the engineering profession.

This final year project especially allowed me to partially master the StarCCM+® calculation software as well as the understanding of the different models, laws and parameters for the simulation of combustion reactions in general which as a future pyrotechnic engineer is of paramount importance. Strong of this experience, I was asked to give a course to the new freshmen recently arrived in the lab to pursue a Master of science in combustion which taught me to build and give an introductory course on a relatively familiar topic while enhancing my language and didactic skills. In addition to the simulation and model building, I was led to manage a campaign of experiments in cooperation with two other students which allowed me to develop my teamwork skills and to conduct experiments involving hazardous substances in a fully autonomous way.

From a cultural point of view, this internship was an amazing opportunity to discover a Chinese culture country with its peculiarities, customs and mysteries. I used to work in a highly multi-cultural environment involving Taiwanese, Indian, Burkinabe and French partners which allowed me to deeply improve my language skills enhancing my Chinese comprehension but also my English, both written and oral, which was my main professional spoken language during the whole internship. The latter also taught me to cope with my own in an environment deeply different from the European one allowing me to become more mature and independent both professionally and personally.

Table of figures

Table of tables

References

1	"Encyclopédie des gaz Air Liquide" [online], Air Liquide, [accessed the 16th of August 2018], Available on https://encyclopedia.airliquide.com/fr	[Air – 2018]
2	André Bakker, "Lecture 5 – Solution Methods: Applied Computational Fluid dynamics", www.bakker.org, May 2018, 45 pages	[Bak – 2018]
3	"The NASA polynomials" [online], The Combustion Laboratory at the University of California, Berkeley, [accessed 10th April 2018], Available on http://combustion.berkeley.edu/gri_mech/data/nasa_plnm.html	[Ber – 2018]
4	Pierre Boivin, "Reduced-Kinetic Mechanisms for Hydrogen and Syngas Combustion Including Autoignition", *Ph.D. Thesis – Universidad Carlos III de Madrid*, December 2011, 112 pages	[Boi – 2011]
5	J. W. Buddenberg, C. R. Wilke, "Calculation of Gas Mixture Viscosities", *University of California, Berkeley*, December 1948, 1345-1347	[Bud – 1948]
6	Brooks® Instrument, Model 5850E – Mass Flow Controller, *Installation and Operation Manual*, September 2009, 64 pages	[Bro – 2009]
7	Ivan Celanovic, Peter Bermel, Marin Soljacic, "Thermophotovoltaic power conversion systems: current performance and future potential", May 2011, 5 pages	[Cel – 2011]
8	Ismail B. Celik, Urmila Ghia, Patrick J. Roache, Christopher J. Freitas, Hugh Coleman, Peter E. Raad, "Procedure for Estimation and Reporting of Uncertainty due to Discretization in CFD applications", *Journal of Fluids Engineering 130*, 2008, 1-4	[Cel – 2008]
9	CHEMKIN, "CHEMKIN Tutorials Manual", *Reaction Design: San Diego*, 2011, 274 pages	[CHE0 – 2011]
10	CHEMKIN, "The CHEMKIN Thermodynamic Database", *CHEMKIN Collection Release 3.6*, September 2000, 40 pages	[CHE1 – 2000]
11	CHEMKIN, "A Software Package for the Analysis of Gas-Phase chemical and Plasma Kinetics", *CHEMKIN Collection Release 3.6*, September 2000, 181 pages	[CHE2 – 2000]
12	CHEMKIN, "A Software Package for the Analysis of Heterogeneous Chemical Kinetics at a Solid-Surface / Gas-Phase Interface", *CHEMKIN Collection Release 3.6*, September 2000, 170 pages	[CHE3 – 2000]
13	CHEMKIN, "A Software Package for the Evaluation of Gas-phase, Multicomponent Transport Properties", *CHEMKIN Collection Release 3.6*, September 2000, 51 pages	[CHE4 – 2000]
14	Junjie Chen, Longfei Yan, Wenya Song, Deguang Xu, "Kinetic interplay between hydrogen and carbon monoxide in syngas-fuelded catalytic micro-combustors", *International journal of hydrogen energy 42*, 2017, 12681-12695	[Che – 2017]
15	Jared P. Ciferno, John J. Marano, "Benchmarking Biomass Gasification Technologies for Fuels, Chemicals and Hydrogen Production", *U.S. Department of Energy*, National Energy Technology Laboratory, June 2002, 19-20	[Cif – 2002]
16	George D. Cody, "Theoretical Maximum Efficiencies for Thermophotovoltaic devices", *AIP Conference Proceedings 460*, Exxon Corporate Clinton Township, 1999, 11 pages	[Cod – 1999]
17	Copper Development Association, "The Copper Advantage: A guide to working with Copper and Copper Alloys", www.antimicrobialcopper.com, April 2018, 28 pages	[Cop – 2018]
18	Scott G. Davis, Ameya V. Joshi, Hai Wang, Fokion Egolfopoulos, "An optimized kinetic model of H2/CO combustion", *Proceedings of the Combustion Institute 30*, 2005, 1283-1292	[Dav – 2005]
19	Berk Demirgok, Orlando Ugarte, Damir Valiev, V'yacheslav Akkerman, "Effect of thermal expansion on flame propagation in channels with nonslip walls", *Proceedings of the Combustion Institute 35*, 2015, 929-936	[Dem – 2015]
20	O. Deutschmann, L.I. Maier, U. Riedel, A.H. Stroemman, R.W. Dibble, "Hydrogen assisted catalytic combustion of methane on platinum", *Catalysis Today 59*, 2000, 141-150	[Deu – 2000]
21	E4Tech, "Review of Technologies for Gasification of Biomass and wastes", *NNFCC project*, September 2008, 130 pages	[E4T – 2008]
22	"Standard Grade Coal – Heating Values" [online], The Engineering Toolbox, [accessed the 16th of August 2018], Available on https://www.engineeringtoolbox.com/coal-heating-values-d_1675.html	[Eng – 2018]

23 Lewis Fraas, Mitch Groeneveld, Galen Magendanz, Paul Custard, "A single TPV cell power density and efficiency measurement technique", *AIP Conference Proceedings 460,* JX Crystals Inc., 1999, 6 pages [Fra – 1999]

24 Yohannes Ghermay, John Mantzaras, Rolf Bombach, "Experimental and numerical investigation of hetero-/homogeneous combustion of $CO/H_2/O_2/N_2$ mixtures over platinum at pressures up to 5 bar", *Proceedings of the Combustion Institute 33,* 2011, 1827-1835 [Ghe – 2011]

25 D. G. Gritton, R. C. Bourke, "Radioisotope-photovoltaic Energy Conversion System", *Advanced Energy Conversion 5,* 1965, 119–145 [Gri – 1965]

26 Arthur Gutkowski, Luigi Tecce, Jozef Jarosinski, "Flame quenching by the wall-fundamental characteristics", *Journal of KONES Powertrain and Transport 14 n°3,* 2007, 8 pages [Gut – 2007]

27 Ed Horne, "Hybrid Thermophotovoltaic Power Systems", *California Energy Commission – Consultant report,* 22th April 2002, 176 pages [Hor – 2002]

28 "IFA - Institute for Occupational Safety and Health of the German Social Accident Insurance" [online], GESTIS Substance Database, [accessed the 16th of August 2018], Available on http://gestis-en.itrust.de/nxt/gateway.dll/gestis_en/531331.xml?f=templates$fn=default.htm$3.0 [IFA – 2018]

29 Niket S. Kaisare, Dionisios G. Vlachos, "A review on microcombustion: Fundamentals, devices and applications", *Progress in Energy and Combustion Science 38,* 2012, 321-359 [Kai – 2012]

30 Robert J. Kee, Fran M.Rupley, and James A. Miller, "CHEMKIN-III: A Fortran Chemical Kinetics Package for the Analysis of Gas-Phase Chemical and Plasma Kinetics", *Sandia Report* SAND96-8216.UC-405, May 1996, 166 pages [Kee – 1996]

31 Steven Kerampran, "Théorie de la combustion", *ENSTA Bretagne,* 2018, 154 pages [Ker – 2018]

32 Kyu Tae Kim, Dae Hoon Lee, Sejin Kwon, "Effects of thermal and chemical surface-flame interaction on flame quenching", *Combustion and Flame 146,* May 2006, 19-28 [Kim – 2006]

33 J. Koop, O. Deutschmann, "Detailed surface reaction mechanism for Pt-catalyzed abatement of automotive exhaust gases", *Applied Catalysis B: Environmental 91,* 2009, 47-58 [Koo – 2009]

34 F. J. Krieger, "Calculation of the viscosity of gas mixtures", *US Air Force RM-649,* July 1951, 17 pages [Kri – 1951]

35 Dae Hoon Lee, "Scale effects on combustion phenomena in a micro-combustor", *Microscale Thermophysical Engineering 7,* 2003, 235-251 [Lee – 2003]

36 Z.W. Li, S.K. Chou, C. Shu, W.M. Yang, "Effects of step height on wall temperature of a micro-combustor", *Journal of Micromechanics and Microengineering 15,* 2005, 207-212 [Li – 2005]

37 Juan Li, Zhenwei Zhao, Andrei Kazakov, Marcos Chaos, Frederick L. Dryer, James J. Scire Jr, "A Comprehensive Kinetic Mechanism for CO, CH2O and CH3OH Combustion", *International Journal of Chemical Kinetics 39,* 2007, 109-136 [Li – 2007]

38 J. Li, S.K. Chou, W.M. Yang, Z.W. Li, "Experimental and numerical study of the wall temperature of cylindrical micro-combustors", *Journal of Micromechanics and Microengineering 19,* 2008, 11 pages [Li – 2008]

39 Yueh-Heng Li, Guan-Bang Chen, Fang-Hsien Wu, Tsarng-Sheng Cheng, Yei-Chin Chao, "Combustion characteristics in a small-scale reactor with catalyst segmentation and cavities", *Proceedings of the Combustion Institute 34,* 15th September 2012, 2253-2259 [Li – 2012]

40 Yueh-Heng Li, Guan-Bang Chen, Tsarng-Sheng Cheng, Yean-Ling Yeh, Yei-Chin Chao, "Combustion characteristics of a small-scale combustor with a percolated platinum emitter tube for thermophotovoltaics", *Energy 61,* 4th September 2013, 150-157 [Li – 2013]

41 Yueh-Heng Li, Hong-Yuan Li, Derek Dunn-Rankin, Yei-Chin Chao, "Enhancing Thermal, Electrical Efficiencies of a Miniature Combustion-Driven Thermophotovoltaic System", *Progress in photovoltaics: Research and applications 17,* May 2009, 502-512 [Li – 2009]

42 John Mantzaras, "Catalytic Combustion of Syngas", *Combustion Sciences and Technologies 180,* 2008, 1137-1168 [Man – 2008]

43 Ashish Mhadeshwar, Niket Kaisare, "A tutorial on Chemkin", *Indian Institute of Technology of Madras,* December 2007, 15 pages [Mha – 2007]

44	M. A. Mueller, R. A. Yetter, F. L Dryer, "Flow Reactor Studies and Kinetic Modeling of the H_2/O_2/NOx and CO/H_2O/O_2/NOx Reactions", *International Journal of Chemical Kinetics 31*, 1999, 705-724	[Mue – 1999]
45	"WebBook de Chimie NIST" [online], NIST-National Institute of Standards and Technology, US Department of Commerce, [accessed the 16th of August 2018], Available on https://webbook.nist.gov/chemistry/form-ser/	[NIS – 2018]
46	"Flame Quenching in SI Engines" [online], NPTEL (National Programme on Technology Enhanced Learning), [accessed the 16th of August 2018], Available on http://nptel.ac.in/courses/112104033/lecture8/8_2.htm	[NPT – 2018]
47	Pascale Ouimette, "Caractérisation expérimentale et numérique de la flamme de carburants synthétiques gazeux", *Ph.D. Thesis – Ecole de technologie supérieure du Québec*, January 2012, 196 pages	[Oui – 2012]
48	O. Reynolds, "On the Theory of Lubrification and its Application to Mr. Beauchamp Tower's Experiments, including an experimental Determination of the Viscosity of Olive Oil", *Philosophical Transactions of the Royal Society of London 177*, 1886, 157 - 234	[Rey – 1886]
49	Marco Schultze, John Mantzaras, Felix Grygier, Rolf Bombach, "Hetero-/homogeneous combustion of syngas mixtures over platinum at fuel-rich stoichiometries and pressures up to 14 bar", *Proceedings of the Combustion Institute 35*, 2015, 2223-2231	[Sch – 2015]
50	Christopher J. Seeton, "Viscosity-temperature correlation for liquids", *Tribology Letters 22*, 2006, 67-78	[See – 2006]
51	"GRI-Mech 3.0 Homogeneous mechanism" [online], Gregory P. Smith, David M. Golden, Michael Frenklach, Nigel W. Moriarty, Boris Eiteneer, Mikhail Goldenberg, C. Thomas Bowman, Ronald K. Hanson, Soonho Song, William C. Gardiner Jr., Vitali V. Lissianski, Zhiwei Qin, [accessed the 16th of August 2018], Available on http://www.me.berkeley.edu/gri_mech/	[Smi – 2018]
52	Siemens CD-adapco, "Star-CCM+® Documentation Version 11.04", 2016	[Sta – 2016]
53	Joseph Shepherd, "The CHEMKIN / NASA thermo data file" [online], Aeronautics and Mechanical Engineering, California Institute of Technology - Caltech, [accessed 8th May 2018], available on http://shepherd.caltech.edu/EDL/public/thermo.html	[She – 2018]
54	Ran Sui, Et-touhami Es-sebbar, John Mantzaras, Nikolaos I. Prasianakis, "Experimental and Numerical Investigation of Fuel-Lean H2/CO/Air and H2/CH4/Air Catalytic Microreactors", *Combustion Sciences and Technology 190*, 2017, 336-362	[Sui – 2017]
55	Hongyan Sun, S.I. Yang, G. Jomaas, C.K. Law, "High-pressure laminar flame speeds and kinetic modelling of carbon monoxide/hydrogen combustion", *Proceedings of the Combustion Institute 31*, 2007, 439-446	[Sun – 2007]
56	Chih-Jen Sung, Chung K. Law, "Fundamental Combustion Properties of H2/CO Mixtures: Ignition and Flame Propagation at Elevated Pressures", *Combustion Science and Technology 180*, 2008, 1097-1116	[Sung – 2008]
57	W. Sutherland, "The viscosity of gases and molecular force", *Philosophical Magazine Series 5*, 1893, 507-531	[Sut – 1893]
58	Unknown, "Chapter 8 – Flow in Pipes", *Fluid Mechanics*, 2004, 321-343	[Unk - 2004]
59	"Gasification Introduction" [online], US Department of Energy, [accessed the 16th of August 2018], Available on https://www.netl.doe.gov/research/coal/energy-systems/gasification/gasifipedia/syngas-composition	[USD – 2018]
60	Lars Waldheim, Torbjörn Nilsson, "Heating value of gases from biomass gasification", *IEA Bioenergy Agreement, Task 20 – Thermal Gasification of Biomass*, May 2001, 61 pages	[Wal – 2001]
70	Zhe Wang, Jinning Yang, Zheng Li, Yong Xiang, "Syngas composition study", *Front. Energy Power Engineering China 3*, 2009, 369-372	[Wan – 2009]
71	J. Warnatz, "Rate coefficients in the C/H/O system", *Gas Phase Combustion Chemistry*, W.C. Gardiner Jr., 1984, 197-360	[War1 – 1984]
72	J. Warnatz, U. Maas, R.W. Dibble, "Combustion: Physical and Chemical Fundamentals, Modeling and Simulation, Experiments, Pollutant Formation", *4th Edition Springer Berlin Heidelberg New-York*, 2006	[War2 – 2006]
73	C. R. Wilke, "A viscosity Equation for Gas Mixtures", *The Journal of Chemical physics 18*, April 1950, 517-521	[Wil – 1950]
74	Chui Hong Wong, Wan Sia Heng, Lai Wah Chan, "Viscosity-temperature relationship of liquid-based excipients amenable for spray congealing: Derivation of a rheological parameter with good correlation to particle size", *European Journal of Lipid Science and Technology 118*, 2016, 1062-1073	[Won – 2016]

75	Yu-Ting Wu, Yueh-Heng Li, "Combustion characteristics of a micro segment platinum tubular reactor with a gap", *Chemical Engineering Journal 304,* 22nd June 2016, 485-492	[Wu – 2016]
76	W.M. Yang, S.K. Chou, C. Shu, H. Xue, Z.W. Li, D.T. Li, J.F. Pan, "Microscale combustion research for application to micro thermophotovoltaic systems", *Energy Conversion and Management 44*, December 2002, 2625-2634	[Yan – 2002]
77	W.M. Yang, S.K. Chou, J.F. Pan, J. Li, X. Zhao, "Comparison of cylindrical and modular micro-combustor radiators for micro-TPV system application", *Journal of Micromechanics and Microengineering 20*, 22 June 2010, 1-8	[Yan – 2010]
78	R.A. Yetter, F.L. Dryer, H. Rabitz, "A comprehensive Reaction Mechanism for carbon monoxide/hydrogen/oxygen kinetics", *Combustion Science and Technology 79*, 1991, 97-128	[Yet – 1991]
79	Harun Yilmaz, Omer Cam, Ilker Yilmaz, "Effect of micro combustor geometry on combustion and emission behaviour of premixed hydrogen/air flames", *Energy 135*, 30th June 2017, 585-597	[Yil – 2017]
80	Matthias Zenker, Andreas Heinzel, Gunther Stollwerck, Jorg Ferber, Joachim Luther, "A single TPV cell power density and efficiency measurement technique", *AIP Conference Proceedings 460,* JX Crystals Inc., 1999, 6 pages	[Zen – 1999]
81	Xin Zheng, Marco Schultze, John Mantzaras, Rolf Bombach, "Effects of hydrogen addition on the catalytic oxidation of carbon monoxide over platinum at power generation relevant temperatures", *Proceedings of the Combustion Institute 34*, 2013, 3343-3350	[Zhe – 2013]
82	Xin Zheng, John Mantzaras, Rolf Bombach, "Kinetic interactions between hydrogen and carbon monoxide oxidation over platinum", *Combustion and flame 161*, 2014, 332-346	[Zhe – 2014]